


Article

A Comparative Study of Different Sorbents in the Context of Direct Air Capture (DAC): Evaluation of Key Performance Indicators and Comparisons

Grazia Leonzio , Paul S. Fennell and Nilay Shah

Department of Chemical Engineering, Imperial College London, South Kensington, London SW7 2AZ, UK; p.fennell@imperial.ac.uk (P.S.F.); n.shah@imperial.ac.uk (N.S.)

* Correspondence: g.leonzio20@imperial.ac.uk

Abstract: Direct air capture can be based on an adsorption system, and the used sorbent (chemisorbents or physisorbents) influences process. In this work, two amine-functionalized sorbents, as chemisorbents, and three different metal organic frameworks, as physisorbents, are considered and compared in terms of some key performance indicators. This was carried out by developing a mathematical model describing the adsorption and desorption stages. An independent analysis was carried out in order to verify data reported in the literature. Results show that the equilibrium loading is a critical parameter for adsorption capacity, energy consumption, and cost. The considered metal organic frameworks are characterized by a lower equilibrium loading (10^{-4} mol/kg) compared to chemisorbents (10^{-1} mol/kg). For this reason, physisorbents have higher overall energy consumptions and costs, while capturing a lower amount of carbon dioxide. A reasonable agreement is found on the basis of the operating conditions of the Climeworks company, modelling the use of the same amine cellulose-based sorbent. The same order of magnitude is found for total costs (751 USD/tonneCO₂ for our analysis, compared to the value of 600 USD/tonneCO₂ proposed by this company).

Keywords: metal organic frameworks; amine-functionalized sorbents; DAC; adsorption; key performance indicators



Citation: Leonzio, G.; Fennell, P.S.; Shah, N. A Comparative Study of Different Sorbents in the Context of Direct Air Capture (DAC): Evaluation of Key Performance Indicators and Comparisons. *Appl. Sci.* **2022**, *12*, 2618. <https://doi.org/10.3390/app12052618>

Academic Editor: Nikolaos Koukoulas

Received: 26 January 2022

Accepted: 1 March 2022

Published: 3 March 2022

Publisher's Note: MDPI stays neutral with regard to jurisdictional claims in published maps and institutional affiliations.



Copyright: © 2022 by the authors. Licensee MDPI, Basel, Switzerland. This article is an open access article distributed under the terms and conditions of the Creative Commons Attribution (CC BY) license (<https://creativecommons.org/licenses/by/4.0/>).

1. Introduction

Global warming and climate change are being caused by the increase in greenhouse gases, primarily carbon dioxide (CO₂), in the atmosphere. CO₂ emissions were estimated to be more than 33 Gtons in 2018 [1]. In order to achieve the “2 °C target” proposed by the Intergovernmental Panel on Climate Change (IPCC), CO₂ may need to be captured at a rate of 25 Gt/yr in 2050 [2]. About half of these emissions are due to diffuse sources, belonging to the transport sector and small sources (homes and offices) [3].

CO₂ can be captured by using a negative emission technology such as Direct Air Capture (DAC), proposed first as a mitigation option by Lackner in 1999 [4–6]. By using this technology, the captured CO₂ can be verifiably removed from the atmosphere. Potential technologies include Direct Air Carbon Capture and Storage (DACCS) processes, or the CO₂ could potentially be used in a Direct Air Carbon Capture and Utilization (DACCU) system [7–9].

Direct Air Capture technologies might include absorption, adsorption, mineral carbonation, membrane, photocatalysis, cryogenic separation, electrochemical approaches, and electro dialysis [4,10–15]. However, among these, absorption and adsorption are the most mature and most investigated in the literature [4].

For defined advantages of adsorption system, potential applications for CO₂ capture using this technology are growing significantly and this work is focused on this technology addressing the relative merits of different sorbents (among physisorbents and

chemisorbents), from a performance point of view, regarding capacity, energy efficiency, and economic viability [16,17].

For physisorption, only a physical interaction occurs between CO₂ and surface sorbent, weak Van Der Waals forces are established, and low CO₂ adsorption capacities are exhibited, owing to the relatively low adsorption heat [18]. Potential sorbents include zeolites, activated carbons, metal-organic frameworks (MOFs), and other new materials (e.g., boron nitride nanosheets and nanotubes) [10,19].

Particular interest has recently been paid towards MOFs, as underlined by publications growing rapidly in the last decade [20–26]. In fact, MOFs have a specific surface area much higher than other porous materials such as activated carbons and zeolites with values up to 7140 m²/g [27,28].

Chemisorption involves a chemical reaction between CO₂ and surface sorbent, for example, an amine functionalized sorbent, making the CO₂ capture capacity larger [29,30]. Amine-functionalized sorbents are divided in three different classes [4]. In class I, there is a physical impregnation of amines on a porous support. In class II, amines are covalently bonded on the walls of porous support, while in class III, amine monomers are polymerized in situ, resulting in a polyamine structure bonded to the walls of support.

Chemisorbents are investigated in more detail than MOFs for air capture, due to their high uptake capacity and selectivity, resilience to humidity (which has a positive effect on CO₂ capture), and the possibility of regeneration under relatively mild conditions [3,10].

Generally, research in this field has explored and optimized adsorption capacities, kinetics and regenerability for amine-functionalized sorbents individually [31–36] and this is also the case for MOFs [37–41].

Experimentally, as shown in Table 1, it has been found that for amine-based sorbents of class I, CO₂ uptakes can be up to 3.36 molCO₂/kg of sorbent for a polyethylenimine (PEI) functionalized hierarchical bimodal meso/microporous silica support in the presence of 19% of relative humidity [32]. A mixture of PEI and poly(ethylene glycol) (PEG) impregnated on a fumed silica support has been reported in Meth et al. [42] with an adsorption capacity of 6.8×10^{-1} molCO₂/kg. Brillman and Veneman [43] considered a mixture of tetraethylenepentamine (TEPA) and PEI, obtaining a CO₂ uptake of 2.5 molCO₂/kg, using temperature swing adsorption for regeneration. Other amines which have been investigated are: poly(propylenimine) (PPI) [33,44] and poly(allylamine) (PAA) [45].

For amine-based sorbents of class II, CO₂ uptakes of up to 2.13 molCO₂/kg and 3.89 molCO₂/kg have been obtained, respectively for 3-aminopropylmethyldiethoxysilane (APDES) grafted onto nanofibrillated cellulose (NFC) [46] and hydrazine (H₂N₄) onto Mg₂(dobpdc) [47]. Good adsorption capacities are also reported in the work of Belmabkhout et al. [30], Ng et al. [48], and Choi et al. [40], respectively of 1.4 molCO₂/kg for triaminesilane (TRI) onto MCM-41, 1.39 molCO₂/kg for N-(2-aminoethyl)-3-aminopropylmethyl dimethoxysilane (AEAPDMS) onto NFC and 1.5 for ethylenediamine (ED) grafted onto Mg/DOBDC.

Lower CO₂ uptakes are measured for amine-functionalized sorbents of class III. In total, 1.78 molCO₂/kg and 1.68 molCO₂/kg are shown in the work of Choi et al. [49] and Abhilash et al. [36]. In the first case, aziridine is considered with silica support, while in the second case, 3-aminopropyl triethoxysilane (APTMS) is evaluated in hybrid silica material.

Similar experimental analyses have been carried out for MOFs, showing adsorption capacities to be lower compared to those of amine-based sorbents, as in Table 2. Capacities of 0.18 molCO₂/kg for SIFSIX-3-Ni [50], 0.05 molCO₂/kg for HKUST-1 [39], and 0.14 for Mg-MOF-74 [51] have been measured.

Table 1. CO₂ uptakes of some amine-functionalized sorbents.

Support	Amine	Conditions	Con. CO ₂ (ppm)	Adsorption Capacity (molCO ₂ /kg _{sorbent})	Reference
Class I					
Hierarchical bimodal meso/microporous silica	PEI	303 K, 19% relative humidity	400	3.36	Kwon et al. [28]
Fumed silica	PEI + PEG	323 K	360	6.8×10^{-1}	Meth et al. [38]
Silica and polymethylmethacrylate	TEPA	308 K	400	2.50	Brilman and Veneman [39]
SBA-15	PPI prepared by HClO ₄	303 K	400	3.1×10^{-1}	Sarazen et al. [29]
SBA-15	PPI prepared by HBr	303 K	400	2.5×10^{-1}	Sarazen et al. [29]
SBA-15	PPI prepared by HCl	303 K	400	1.5×10^1	Sarazen et al. [29]
SBA-15	PPI prepared by CH ₃ SO ₃ H	303 K	400	1.7×10^{-1}	Sarazen et al. [29]
Microporous polymer	PEI	308 K	400	2×10^{-1}	Pang et al. [40]
Mesocellular foam	PAA	298 K	400	6.3×10^{-1}	Chaikittisilp et al. [41]
Mesocellular foam	PEI	298 K	400	6.1×10^{-1}	Chaikittisilp et al. [41]
Mesocellular foam	PEI	298 K	400	4.4×10^{-1}	Chaikittisilp et al. [41]
Class II					
Nanofibrillated cellulose	APDES	296 K, relative humidity	400	2.13	Gebald et al. [42]
Mg ₂ (dobpdc)	H ₂ N ₄	298 K	400	3.89	Liao et al. [43]
MCM-41	TRI	298 K, 67% relative humidity	300	1.40	Belmabkhout et al. [26]
Nanofibrillated cellulose	AEAPDMS	298 K, 40% relative humidity	506	1.39	Ng et al. [44]
Mg/DOBDC	ED	298 K	400	1.50	Choi et al. [36]
Class III					
SBA-15	Aziridine	298 K	400	1.78	Choi et al. [45]
Hybrid silica materia	APTMS	303 K, relative humidity	400	1.68	Abhilash et al. [32]

Table 2. Adsorption capacity of some physisorbents from ambient air at 49% of relative humidity.

Physisorbent	Adsorption Capacity (mol/kg _{sorbent})		Reference
	CO ₂	H ₂ O	
SIFSIX-3-Ni	1.8×10^{-1}	5.17	Shekhah et al. [50]
HKUST-1	5×10^{-2}	9.89	Kumar et al. [39]
Mg-MOF-74	1.4×10^{-1}	9.50	Caskey et al. [51]

These experimental analyses are complemented by mathematical models, which are able to replicate the process cycles, explore operating conditions not investigated in experimental work, and save time and cost for screening, development, and optimization [52]. More importantly, modeling can carry out economic and energetic analysis to evaluate costs and energy consumption, including the thermal energy required for the desorption stage and the electrical energy for fans blowing air through the air sorbent contactor.

Moreover, other key performance indicators (KPIs) can also be evaluated by using mathematical models, with the aim to compare, screen, and select the best scenarios.

Estimates of costs and energy consumptions for main DAC technologies, and in particular for adsorption systems are reported by Fasihi et al. [53]. Here, electricity requirements can range between 150 and 300 kWh_{el}/tonneCO₂ for amine-based sorbents, and up to 1420 kWh_{el}/tonneCO₂ for MOFs. On the other hand, thermal energy of between 1170 and 2000 kWh_{th}/tonneCO₂ is required. Regarding costs for adsorption, as reported in Table 3, Fasihi et al. [53] suggest a value between 63 and 86 USD/tonneCO₂ obtainable by 2040.

Table 3. Estimated costs for adsorption technology.

Literature Work/Team	Actual Cost (USD/tonneCO ₂)	Future Cost (USD/tonneCO ₂)
Fasihi et al. [53]		6.3×10^1 – 8.6×10^1
Kulkarni and Sholl [54]	4.3×10^1 – 4.94×10^2	
Zhang et al. [18]	9.1×10^1 – 2.27×10^2	
Sinha et al. [55]	6×10^1 – 1.9×10^2	
Viebahn [56] (Climeworks)	6×10^2	1×10^2
Kintisch [57] (Global Thermostat)		1.5×10^1 – 5×10^1

The expected cost for the technology in the future is lower than those evaluated by others in the literature for the present day. Kulkarni and Sholl [54] report a cost of CO₂ capture of 43–494 USD/tonneCO₂, while Zhang et al. [18] suggest a cost between 91 and 227 USD/tonneCO₂ (not including capital costs for equipment). Sinha et al. [55] estimate a cost of capture of 60–190 USD/tonneCO₂ (without discounting cash flows, and assuming a self-contained sorbent). However, these analyses reported in the literature are conducted with different assumptions for energy inputs, different output conditions (pressure and CO₂ purity), and without transparency [53].

Estimates provided by companies are also present in the literature. Generally, these companies suggest a low cost, but such estimates need to be considered in the context that the companies are in the process of commercializing the technology [2]. Climeworks is expecting to reduce the cost from 600 USD/tonneCO₂ to 100 USD/tonneCO₂ by 2030, while a more optimistic forecast is proposed by Global Thermostat, with suggested costs of 15–50 USD/tonneCO₂ for the near future [53]. Such costs appear to be unrealistic.

From the considered literature analysis, it is evident that there is a gap to conduct an independent and complete analysis to evaluate some important KPIs, such as costs (operating and capital) and energy consumption of a number of important DAC technologies, including chemisorption and physisorption, based on the design of DAC process. Of the two, physisorption has hitherto received less attention from the research community.

The work of Sabatino et al. [58] reports a comparison between some MOFs and amine-functionalized sorbents to evaluate costs and energy consumptions; however, their research is not based on design calculation but multi-objective optimization without any correlation between design parameters. Other research on adsorption technology are concerned with the sensitivity analysis of operating parameters [59,60], regeneration methodology [61], new adsorbent bed [62], and thermodynamics [63].

This proposed work, following a design procedure, compares the theoretical performance and techno-economics of two amine-functionalized sorbents, SI-AEATPMS ([N-(2-aminoethyl)-3-aminopropyl]trimethoxysilane (AEATPMS) grafted on silica gel) and APDES-NFC-FD (3-aminopropylmethyl-diethoxysilane (APDES) on nanofibrillated cellulose (NFC)), in addition to three different MOFs (MIL-101, MOF-177, MOF-5), with the aim to capture CO₂ from dry air, by using an adsorption system based on temperature swing for regeneration.

We are supposing conditions without the relative humidity of air due to limitations in the literature data for the selected sorbents. In any case, this assumption reduces the energy consumption of the desorption stage for chemisorbents and to ensure a higher capture efficiency for physisorbents.

SI-AEATPMS and APDES-NFC-FD are considered because they were suggested by the Climeworks company for DAC systems. MOF-5, MOF-177, and MIL-101 are taken into account because they have already been used in the literature for carbon dioxide capture with good performances and advantages compared to other sorbents (high adsorption capacity, thermally stable, and good strength to withstand pressures) [64,65]. As the most investigated in the literature and in real applications for CO₂ capture, these sorbents can provide a good representation of the whole families of sorbents. The chemisorbents and physisorbents are analyzed and compared in terms of the previously mentioned KPIs (electricity and thermal energy consumption, costs and amount of CO₂ captured or CO₂ productivity), and against data provided by the Climeworks company for the first “commercial” plant in the world, used as a case study. The defined KIPs are chosen because they suggest the techno-economic feasibility of the process. A mathematical model describing the adsorption and desorption stage is developed, to allow an independent analysis.

2. Mathematical Modelling

2.1. Sorbents and Adsorbent Bed

Here, the MOFs (MIL-101, MOF-5 and MOF-177) (physisorbents) are compared against two amine-functionalized chemisorbents which have been suggested by Climeworks to be of interest. In particular, the APDES-NFC-FD sorbent is used by this company in its plant located in Switzerland. These amine-based sorbents are: SI-AEATPMS ([N-(2-aminoethyl)-3-aminopropyl]trimethoxysilane (AEATPMS) grafted on silica gel) and APDES-NFC-FD (3-aminopropylmethyl-diethoxysilane (APDES) onto nanofibrillated cellulose (NFC)), both belonging to class 2.

MOFs are considered because of their high porosity, ordered and well-characterized porous structures, and adjustable chemical functionality which makes them potentially very attractive for CO₂ adsorption [66]. These properties are purported to allow them to capture and release CO₂ with fast kinetics and high reversibility over many cycles. Little data are present in the literature about CO₂ capture using these kinds of sorbents. In contrast, amine-functionalized sorbents are selected for study because their strong bonds with CO₂ allow significant uptake at low CO₂ partial pressure [4].

The selected sorbents are produced through synthesis routes described in the literature, as follows.

The synthesis of MOF-5 starts with a reaction between Zn(NO₃)₂·6H₂O and 1,4 benzene dicarboxylic acid in N,N'-dimethylformamide solvent at 373 K [67]. After cooling, the mother liquor was decanted from the crystalline material, and the white solid was washed with dimethylformamide [68]. Properties such as the BET specific surface area, average par-

ticle size, and micropore volume have been evaluated and reported by Zacharia et al. [69], and are respectively $3570 \text{ m}^2/\text{g}$, $2 \text{ }\mu\text{m}$, and $1.25 \text{ cm}^3/\text{g}$.

MOF-177 can be obtained through a room temperature technique, mixing benzenetribenzoic acid and zinc acetate dehydrate with diethylformamide. The obtained compound was filtered, washed with diethylformamide, then chloroform was added to remove impurities. After that, the MOF was thermally activated under vacuum at 393 K [70]. Pore textural properties were provided by Saha and Deng [71]: BET specific surface area, pore diameter, and pore volume are, respectively, $1218 \text{ m}^2/\text{g}$, 14.4 \AA , and $0.748 \text{ cm}^3/\text{g}$.

For the synthesis of chromium terephthalate metal–organic framework (MIL101) a mixture of benzene-1,4-dicarboxylic acid, chromium(III) nitrate nonahydrate, hydrogen fluoride, and water was heated at 493 K, forming a green crystalline powder. After a natural cooling, the obtained material was filtered to separate the MIL-101 powder [72]. This MOF is characterized by a high BET surface area ($>3000 \text{ m}^2/\text{g}$), a large pore diameter ($29\text{--}34 \text{ \AA}$), and a huge pore volume ($\approx 2 \text{ cm}^3/\text{g}$) [73].

The SI-AEATPMS sorbent has been synthesized by drying silica gel beads inside a natural convection oven at 383 K, before loading with AEATPMS, in a two-neck flask equipped with a reflux condenser. The mixture was heated at 423 K in a silicone oil bath for 3 h. After cooling to 298 K, the solid product was washed in diethyl ether, and dried in ambient air for 24 h [74]. BET surface area, pore volume, and average pore size were $216 \text{ m}^2/\text{g}$, $0.65 \text{ cm}^3/\text{g}$, and 9.6 nm .

The other amine-functionalized sorbent, APDES-NFC-FD, has been obtained by adding APDES to NFC hydrogel to obtain a suspension of 10% *w/w* of APDES, and incubated for 2 h. This compound was then added dropwise into liquid N_2 to produce a freeze-dried frozen granulate. The obtained material was then subjected to thermal treatment at 393 K under N_2 flow in a natural convection oven. The final grains had a BET surface area of $12.2 \text{ m}^2/\text{g}$, [75].

Data regarding particle and density diameter, and bed porosity for the considered MOFs are reported in Table 4, while the same parameters for amine-based sorbents are shown in Table 5.

Table 4. Main data for MOFs.

MIL 101			
Particle diameter	3.8×10^{-3}	m	Eyitope [75]
Particle density	6.2×10^2	kg/m^3	Ferey et al. [72]
Bed porosity	4.4×10^{-1}		
MOF-177			
Particle diameter	3.8×10^{-3}	m	Eyitope [75]
Particle density	4.3×10^2	kg/m^3	Kaskel [76]
Bed porosity	4.4×10^{-1}		Qasem et al. [64]
MOF-5			
Particle diameter	3.8×10^{-3}	m	Eyitope [75]
Particle density	6.21×10^2	kg/m^3	Qasem et al. [64]
Bed porosity	4.4×10^{-1}		

Table 5. Main data for amine-functionalized sorbents.

SI-AEATPMS			
Particle diameter	2×10^{-3}	m	Goyal et al. [77]
Particle density	1.31×10^3	kg/m ³	Goyal et al. [77]
Bed porosity	6×10^{-1}		
APDES-NFC-FD			
Particle diameter	5×10^{-3}	m	Wurzbacher [73]
Particle density	5.54×10^1	kg/m ³	Wurzbacher [73]
Bed porosity	5×10^{-1}		

For the air contactor, the assumptions in Table 6 are made, based on those reported by Climeworks [78]. The company has a plant with 18 adsorbent unit beds, 3 rows of beds with 6 bed units each. At any given time, some collector units are capturing CO₂, while others are releasing CO₂, meaning that the overall plant operates continuously. In this work, we modelled a single-unit adsorbent bed, considering the air flow rate of one collector. Moreover, in the Climeworks plant, the sorbent is arranged in at least two stacked layers [79]. Each layer could be considered as a very short, packed bed. The void fraction takes into account the void between each layer and among particle sorbents. This justifies our assumption to model the air contactor as a packed bed.

Table 6. Data of one adsorbent bed unit.

Area footprint excl. options	2×10^1	m ²
Height	3.2	m
CO ₂ flow rate, inlet	1.8×10^2	kg/day
Y _{CO₂} , inlet	4×10^{-4}	
Air flow rate, inlet	2.86	m ³ /s

The single module has an area footprint excl. options of 20 m², with a height of 3.2 m. In total, 180 kg/day of CO₂ are fed with an air flow rate of 2.86 m³/s (the CO₂ concentration in the air is 400 ppm).

2.2. Model Equations

The simulation model is based on a gas phase and adsorbed phase material balance, requiring one partial differential equation and one ordinal differential equation to be taken into account. The Maple tool was used for the solution of this equation system. Overall, the following assumptions are made for the analyzed system: the gas phase follows the idea of gas laws due to the low partial pressure, radial gradients are neglected, the bed is isothermal (due to the low partial pressures and concentrations of the adsorbable component, neglecting heat of adsorption and velocity [80]), constant bed porosity and physical properties, negligible N₂ and H₂O adsorption compared to CO₂ (due to the low partial pressure and ideal conditions, interactions between molecules are neglected, then the adsorption can be considered as a single component, while we are assuming that water is removed before the adsorption as defined above), and the linear driving force (LDF) model is used for adsorption kinetics. Regeneration of the sorbent is conducted by changing the bed temperature, i.e., a Temperature Swing Adsorption (TSA) process, as the scheme in Figure 1.

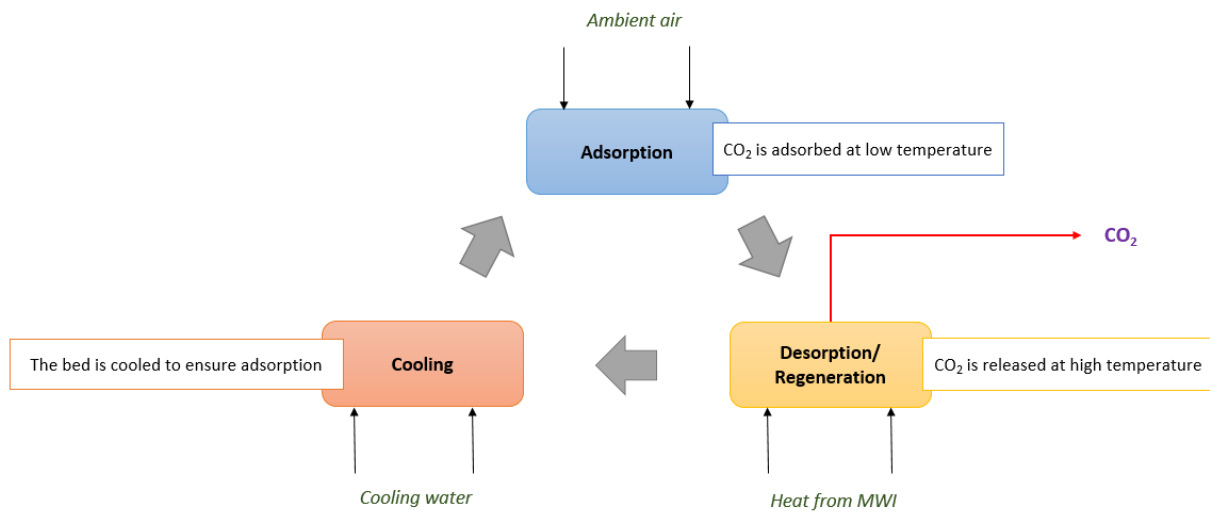


Figure 1. Operating principle of TSA process.

The gas phase material balance for CO₂ is described by the 1D axial dispersed plug flow model, as in the following equation [81] (see Equation (1)):

$$\frac{\partial c_{CO_2}}{\partial t} = -v_{gas} \cdot \frac{\partial c_{CO_2}}{\partial z} + D_z \cdot \frac{\partial^2 c_{CO_2}}{\partial z^2} - \frac{1 - \epsilon}{\epsilon} \cdot \rho_p \cdot \frac{dq}{dt} \quad (1)$$

where D_z is the axial dispersion coefficient (m²/s), z is the axial coordinate (m), v_{gas} is the interstitial gas velocity (m/s), t is time (s), ϵ is the bed void fraction, q is the loading (mol/kg), C_{CO_2} is the CO₂ gas-phase concentration (mol/m³), and ρ_p is the particle density (kg/m³). The axial dispersion coefficient is evaluated by the following correlation [82] (Equation (2)):

$$D_z = (0.45 + 0.55 \cdot \epsilon) \cdot D_m + 0.35 \cdot R_p \cdot v_{gas} \quad (2)$$

with D_m being the molecular diffusivity of CO₂ in air (m²/s), ϵ the bed void fraction, v_{gas} the gas velocity (m/s), and R_p the particle radius (m).

The behavior of the adsorbed phase is described by a linear driving force approximation, as in the following equation [83] (Equation (3)):

$$\frac{dq}{dt} = k_l \cdot (q^* - q) \quad (3)$$

where k_l is the LDF mass transfer coefficient or adsorption time constant (s⁻¹), q^* is the equilibrium adsorbed amount (mol/kg) while q and t are, respectively, the loading (mol/kg) and the time (s) as defined before. According to this approximation, the adsorption rate is proportional to a linear gradient between the adsorbed amount on the sorbent and the amount adsorbed in equilibrium with the bulk concentration [52]. The mass transfer rate is evaluated by the film, microporous and microporous resistances of gases through the porous material as expressed by (see Equation (4)) [27]:

$$\frac{1}{k_l} = \frac{R_p \cdot q_o^*}{3 \cdot k_f \cdot C_o} + \frac{R_p^2 \cdot q_o^*}{15 \cdot \epsilon_p \cdot D_e \cdot C_o} + \frac{r_c^2}{15 \cdot D_c} \quad (4)$$

where, R_p is the particle radius (m), D_c is the diffusivity in the micropore (m²/s), D_e is the effective diffusivity (m²/s), k_f is the film mass-transfer coefficient (m/s), r_c is the microparticle radius (m), ϵ_p is the particle porosity, and q_o^* (mol/m³) is the equilibrium adsorbed phase concentration at the inlet concentration C_o (mol/m³). The film mass transfer coefficient is evaluated from Sherwood number as follows [81] (see Equations (5) and (6)):

$$Sh = 2 + 1.1 \cdot Re^{0.6} \cdot Sc^{0.33} \quad (5)$$

$$k_f = \frac{Sh \cdot D_m}{d_p} \quad (6)$$

where Sh is the Sherwood number, Re is the Reynold number, Sc is the Schmidt number, D_m is the molecular diffusivity (m^2/s), and d_p is the particle diameter (m). The correlation is verified for a range of Reynold number between 3 and 10^4 , with values of dimensionless group in Table S1 of Supporting Information. Using these correlations, the values of k_f for MOF-177 at 298 K and 373 K are, respectively, $1.49 \times 10^{-1} s^{-1}$ and $1.69 \times 10^{-1} s^{-1}$. For MOF-5 this parameter is $0.019 s^{-1}$ at 298 K and $3.3 \times 10^{-2} s^{-1}$ at 373 K. For MIL-101, the adsorption time constant is of $3.3 \times 10^{-2} s^{-1}$ at 298 K and $7.5 \times 10^{-2} s^{-1}$ at 373 K. The SI-AEATPMS sorbent has a value of k_f of $4 \times 10^{-4} s^{-1}$ at 298 K and $5 \times 10^{-4} s^{-1}$ at 383 K, while for the APDES-NFC-FD sorbent the same parameter has a value of $3.8 \times 10^{-3} s^{-1}$ at 298 K and 5.7×10^{-3} at 373 K.

Different adsorption equilibrium isotherms have here been fitted according to the experimental data from the literature at different temperatures.

For MOFs sorbents, equilibrium isotherms are described by the single site Langmuir model [65,75,84] utilizing the following relations (see Equations (7) and (8)):

$$q^* = \frac{q_{sat} \cdot b \cdot P_{CO_2}}{1 + b \cdot P_{CO_2}} \quad (7)$$

$$b = b_0 \cdot e^{-\frac{\Delta H_{CO_2}}{R \cdot T}} \quad (8)$$

with q_{sat} being the maximum adsorbed amount or monolayer capacity (mol/kg), q^* the adsorbed amount in equilibrium (mol/kg), P_{CO_2} the CO_2 partial pressure (bar), b the adsorption constant as a function of temperature (1/bar), R the universal gas constant (J/molK), ΔH_{CO_2} the CO_2 adsorption enthalpy (J/mol), T the temperature (K), and b_0 the adsorption constant at infinite dilution independent of temperature (1/bar). These above data are reported for each MOF in Table 7.

Table 7. Langmuir parameters for MOF sorbents.

MOF-177			
q_{sat}	1.03×10^1	mol/kg	Mason et al. [84]
b_0	2.51×10^{-12}	1/Pa	Mason et al. [84]
ΔH_{CO_2}	-1.4×10^4	J/mol	Qasem et al. [64]
MOF-5			
q_{sat}	4.8×10	mol/kg	Eyitope [75]
b_0	8.06×10^{-10}	1/Pa	Eyitope [75]
ΔH_{CO_2}	-3.4×10^4	J/mol	Eyitope [75]
MIL-101			
q_{sat} (298 K)	3.32×10^1	mol/kg	Montazerolghaem et al. [65]
b (298 K)	3×10^{-2}	1/bar	Montazerolghaem et al. [65]
q_{sat} (373 K)	3×10^{-5}	mol/kg	Montazerolghaem et al. [65]
b (373 K)	7.32×10^2	1/bar	Montazerolghaem et al. [65]
ΔH_{CO_2}	-1.63×10^4	J/mol	Zhang et al. [85]

Equations (7) and (8) are used to describe the adsorption and desorption phases, evolving at two different temperatures: the adsorption is carried out at 298 K, while the desorption takes place at 373 K.

For the SI-AEATPMS sorbent, the adsorption stage, considered at 298 K, is described by the Freundlich isotherm model, as in the following relation [74] (see Equation (9)):

$$q^* = 1.001 \cdot P_{CO_2}^{\frac{1}{8.758}} \tag{9}$$

with P_{CO_2} being the CO₂ partial pressure (bar) and q^* the adsorbed amount in equilibrium (mol/kg). The desorption stage, taking place at 383 K, is, on the other hand, defined (within the literature used) by the Langmuir model as in Equations (7) and (8), with a value for q_{sat} of 0.295 mol/kg and a value for b parameter of 16.1 1/bar [74]. The transition to the Langmuir model from the Freundlich one occurs in the temperature range of 343–383 K, because adsorbate–adsorbate interactions are insignificant above this temperature [86].

The Toth model is used to describe the adsorption and desorption stages, respectively, at 298 K and 373 K, for the APDES-NFC-FD sorbent, as defined in the following correlations [65] (see Equations (10)–(13)):

$$q^* = ns \cdot \frac{b \cdot P_{CO_2}}{\left(1 + (b \cdot P_{CO_2})^t\right)^{\frac{1}{t}}} \tag{10}$$

$$b = b_0 \cdot e^{\frac{\Delta H_{CO_2,0}}{R \cdot T_0} \left(\frac{T_0}{T} - 1\right)} \tag{11}$$

$$ns = ns_0 \cdot e^{\chi \cdot \left(1 - \frac{T}{T_0}\right)} \tag{12}$$

$$t = t_0 + \alpha \cdot \left(1 - \frac{T_0}{T}\right) \tag{13}$$

with P_{CO_2} being the CO₂ partial pressure (bar), q^* the adsorbed amount in equilibrium (mol/kg), T the temperature in K, and $\Delta H_{CO_2,0}$ the negative of the isosteric heat of adsorption at zero fractional loading (J/mol), T_0 the reference temperature of 296 K, ns (mol/kg) and b (1/bar) the constants in the equation, which are a function of temperature, referring, respectively, to the maximum adsorption capacity and adsorption affinity, while t characterizes the system heterogeneity; t_0 , b_0 (1/bar), and ns_0 (mol/kg) are the Toth parameters at the reference temperature, while α and χ are dimensionless constants. Table 8 shows the value of each parameter [74].

Table 8. Toth parameters for APDES-NFC-FD sorbent [74].

b_0	2.25×10^4	1/bar
ΔH_{CO_2}	6×10^4	J/mol
t_0	4.22×10^{-1}	
α	9.49×10^{-1}	
ns_0	1.97	mol/kg
χ	2.37	

To solve the partial differential equation, initial and boundary conditions are first required. For the ordinary differential equation describing the loading only one initial condition is fixed. These boundary conditions are different for the adsorption and desorption stages. For the adsorption stage, the following initial and boundary conditions are considered (see Equations (14)–(16)):

$$c_{CO_2} = q = 0 \quad t = 0 \tag{14}$$

$$c_{CO_2} = c_{CO_2, inlet} \quad z = 0, t > 0 \tag{15}$$

$$\frac{\partial c_{CO_2}}{\partial z} = 0 \quad z = L, t > 0 \tag{16}$$

For the desorption stage, these relations are set as initial conditions (see Equations (17) and (18)):

$$c_{CO_2} = c_{CO_2, inlet} \quad t = 0 \quad (17)$$

$$q = q_{inlet} \quad t = 0 \quad (18)$$

On the other hand, the following boundary conditions are utilized for the regeneration stage (see Equations (19) and (20)) (the supply of CO₂ is stopped during the desorption):

$$c_{CO_2} = 0 \quad z = 0, t > 0 \quad (19)$$

$$\frac{\partial c_{CO_2}}{\partial z} = 0 \quad z = L, t > 0 \quad (20)$$

2.3. Energy Consumption

Energy consumption includes the electrical energy for fans, and the thermal energy for sorbent regeneration. The fan power is calculated by Equation (21) using the Ergun equation as in Equation (22) for the evaluation of pressure drop over the bed [3,80,87] (see Equations (21) and (22)):

$$P_f = \frac{2.72 \cdot 10^{-5} Q \cdot \Delta P}{\mu_f \cdot \mu_m} \quad (21)$$

$$\frac{\Delta P}{L} = \frac{150 \cdot \mu \cdot v_{gas}}{d_p^2} \cdot \frac{(1 - \varepsilon)^2}{\varepsilon^3} + 1.75 \cdot \frac{\rho_{gas} \cdot v_{gas}^2}{d_p} \cdot \frac{(1 - \varepsilon)}{\varepsilon^3} \quad (22)$$

where Q is the fan volume (m³/h), ΔP is the pressure drop (cm of water column in Equation (21) and Pa in Equation (22)), P_f is the fan power (kW), L is the bed height (m), μ is the gas viscosity (Pas), v_{gas} is the gas velocity (m/s), ε is the bed void fraction, ρ_{gas} is the gas density (kg/m³), d_p is the sorbent diameter (m), μ_f is the fan efficiency, and μ_m is the motor efficiency.

Thermal energy for regeneration is evaluated according to Equation (23) [18,88–91]:

$$Q_r = \frac{1}{q_w} \cdot c_{p,s} \cdot (T_{de} - T_{ad}) + \Delta H_{CO_2} \quad (23)$$

where Q_r is the thermal regeneration energy (J/mol), q_w is the working capacity of sorbent, being the difference between the loading at the end of adsorption and desorption stage (mol/kg), $C_{p,s}$ is the specific heat capacity of sorbent (J/kgK), T_{ad} and T_{de} are the adsorption and desorption temperatures, respectively (K), and ΔH_{CO_2} is the absolute value of heat of adsorption (J/mol). The overall thermal energy considers the sensible heat and adsorption heat. The sensible heat required to elevate the adsorbent to the desorption temperature while the second term represents the latent heat needed to break the bond between the carbon dioxide and the adsorbent for regeneration.

2.4. Economic Analysis

Total costs, as the sum of annualized capital (CAPEX) and operating (OPEX) costs, were evaluated according to the procedure suggested by Peter and Timmerhaus for a fluid–solid process type with a detailed factorial estimate [92]. Day zero costs are calculated in terms of fixed capital investment (direct and indirect costs, contractor's fee and contingency) and working capital, while annualized capital costs are evaluated considering a lifetime for the process of 20 years, with an interest rate of 10%. Installation, instrumentation and control, piping, electrical, buildings, yards improvements, service facilities, and land are considered among direct costs and as a percentage of total equipment costs. Engineering and supervision, construction expenses are for indirect costs and as a percentage of total equipment costs.

The equipment costs of an adsorbent bed and fan are calculated from Matches [93], considering carbon steel as the material. The used cost calculator provides an order of

magnitude that is useful for a comparison of different processes as carried out in this work and inputs for the cost evaluation are reported in Table S2 of Supporting Information.

These costs are based on 2014, then are adjusted for inflation using the following correlation adopted from the Chemical Engineering Plant Cost Index (CEPCI) (see Equation (24)) [3]:

$$\frac{Cost_{2021}}{Cost_{2014}} = \frac{CEPCI_{2021}}{CEPCI_{2014}} \quad (24)$$

where the values of $CEPCI_{2014}$ and $CEPCI_{2021}$ are, respectively, 576.1 and 655.9 [94]. A location factor is assumed for CAPEX, assuming that the plant is located in Switzerland. The updated location factor from 1993 [83] to 2021 is 0.58 [84]. OPEX are evaluated as the sum of direct production costs (raw materials and utilities and others as a percentage of capital costs such as maintenance and repairs, operating supplies, patent and royalty), fixed charges (depreciation, local taxes, insurance as a percentage of capital costs), administrative costs, distribution and selling costs, and research and development costs all evaluated as a percentage of the overall production cost.

For the calculation of OPEX, the process is assumed to be fully automated (which indicates that the costs are a base level), while the costs of sorbents, cooling water, waste heat, and electricity are shown in Table 9. Waste heat and electricity are provided by a municipal waste incinerator (MWI), as for the Climeworks plant. The price of MOFs is set to 1.95 USD/kg (the best-case scenario cost for a synthetic sorbent, assuming an efficient scalability of production) while the price of cooling water is of 0.08 USD/m³ [95]. Electricity has a cost of 0.1 USD/kWh [96], while waste heat costs 0.024 USD/kWh [96]. SI-AEATPMS sorbent has a cost of 1.3 USD/kg, while the other, amine-based sorbent has a price of 1.16 USD/kg (these costs are weighted on raw material mass fractions and raw material costs). It is assumed that all adsorbents have a lifetime of 5 years. Currently sorbents used in industry (such as zeolites, activated carbons, and silicas and aluminas) show lifetimes of 7–10 years, while for MOFs a lifetime of 5 years has been defined [95]. For this reason, we are adopting a conservative estimation on the existing knowledge, although the cycle numbers per day can be different among different sorbents.

Table 9. Variable operating costs.

MOF-5	1.95	USD/kg	Danaci et al. [95]
MOF-177	1.95	USD/kg	Danaci et al. [95]
MIL-101	1.95	USD/kg	Danaci et al. [95]
SI-AEATPMS	1.30	USD/kg	
APDES-NFC-FD	1.16	USD/kg	
Cooling water	8×10^{-2}	USD/m ³	Danaci et al. [95]
Electricity from MWI	1×10^{-1}	USD/kWh	Bauer et al. [96]
Waste heat from MWI	2.4×10^{-2}	USD/kWh	SDH [97]

3. Results and Discussion

Firstly, the model was validated by using the experimental data for an adsorber at the lab scale reported in the work of Wurzbacher [74], with the experimental setup as in Figure 2. In this work, CO₂ is captured from air (CO₂ concentration between 400 and 440 ppm) with the SI-AEATPMS sorbent (50 cm³) at 298 K. The air flow rate is of 2×10^{-5} m³/s, with 0–40% of relative humidity. Adsorber diameter and height are 40 mm, ensuring small pressure drops. The steel adsorbent bed is contained in a water bath for heating and cooling, during adsorption and desorption stages. Hot water at 75–95 °C is used for the regeneration stage, while cooling water at 20 °C is used for the cooling stage. All operating conditions are regulated by electronic controllers. At the equilibrium condition, adsorption and desorption times are 24 h and 2 h, respectively.

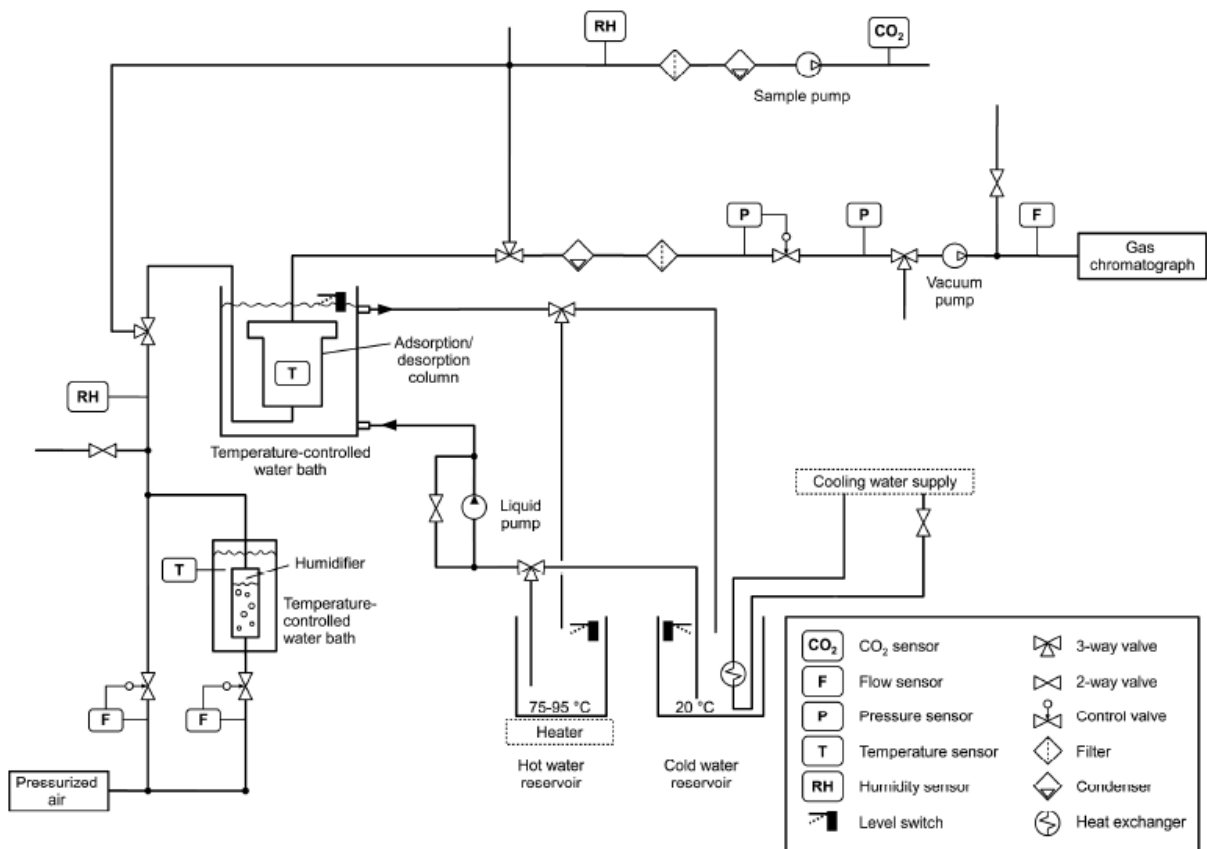


Figure 2. Diagram of the experimental setup used for the validation of the mathematical model [74].

This means that the entire bed is in equilibrium with the feed in about 24 h, as obtained by our mathematical model and shown in the breakthrough curve of Figure S1 in the Supporting Information. This demonstrates good agreement between experimental and simulated results, validating our mathematical model.

3.1. Adsorption and Desorption Curves of DAC Systems

The mathematical model provides the breakthrough curves for the adsorption of CO₂, for the considered chemisorbents and physisorbents. As already mentioned, these plots show the ratio between CO₂ concentration at the bed outlet and the CO₂ feed concentration, as a function of time. Figure 3 shows these trends for MOFs.

Overall, in each Figure, three different sections can be identified as a function of time. At first, the concentration is zero because the step function of CO₂ has not passed the end of the air contactor. After a defined time (the breakthrough time, where the outlet CO₂ concentration rises to 5% of the inlet CO₂ concentration), the concentration increases because CO₂ reaches the end of the adsorber, and the sorbent continues to capture CO₂ until it is in equilibrium with the feed. An adsorption front moves along the bed with time, defining a mass transfer zone. Finally, the sorbent does not capture any more CO₂, because the entire bed is in equilibrium with the CO₂ in the feed. No additional mass transfer occurs between gas and solid phases. This is defined here as the equilibration time (outlet concentration is 95% of the inlet CO₂ concentration) [98]. The difference between breakthrough and equilibration times defines the length of the mass transfer zone. Generally, this value depends on the value of the mass transfer rate: a higher mass transfer rate creates a shorter mass transfer zone [98]. The higher mass transfer rates imply lower mass transfer resistance, and a higher rate of adsorption [99]. Our results show that the shortest mass transfer zone of 146.2 s is present for MOF-177 with the highest mass transfer rate of $1.49 \times 10^{-1} \text{ s}^{-1}$. The greatest mass transfer zone of 703.5 s is present for MOF-5 due

to the lowest mass transfer rate, of $1.9 \times 10^{-2} \text{ s}^{-1}$. On the other hand, for MIL-101 a mass transfer zone of 331.2 s is obtained, for which the value of k_1 is of $3.3 \times 10^{-2} \text{ s}^{-1}$.

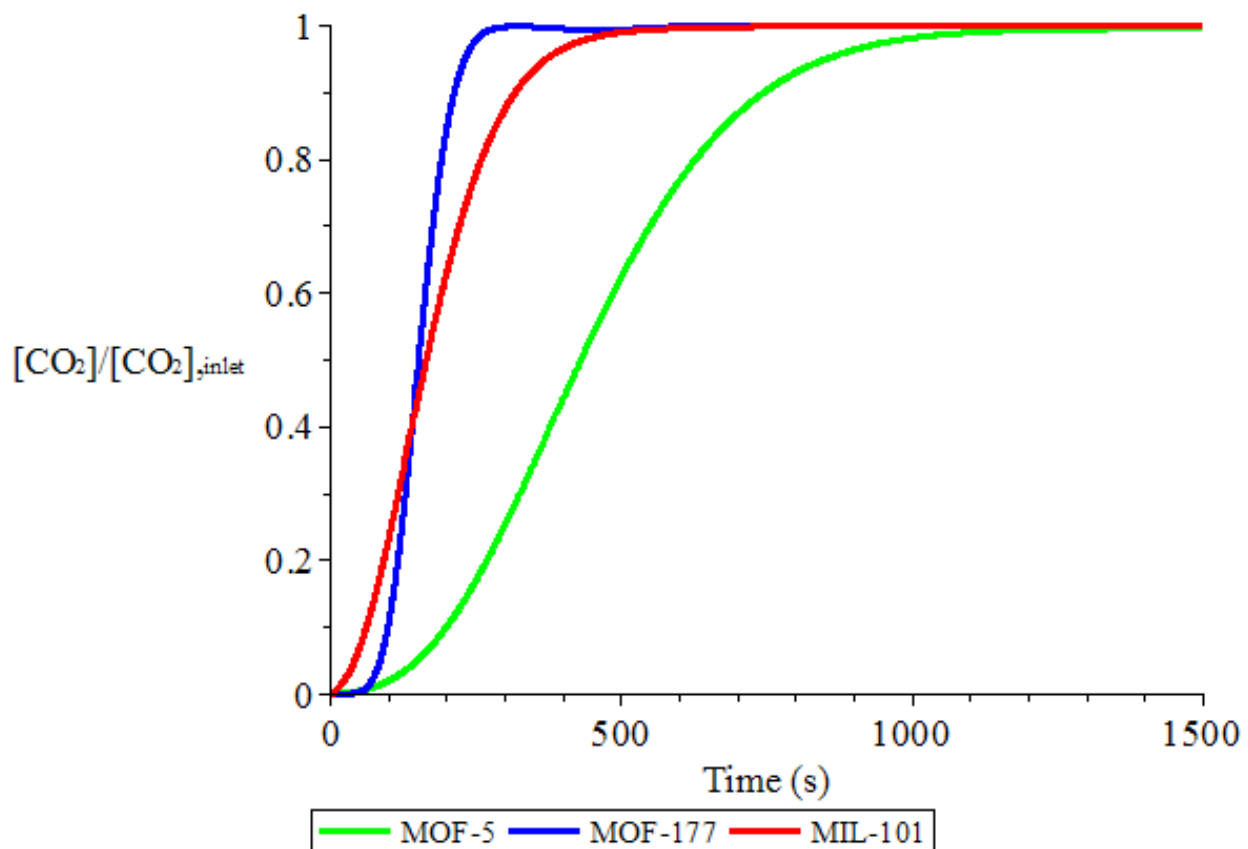


Figure 3. Breakthrough curves (CO_2 concentration at the outlet/ CO_2 concentration at the inlet) for physisorbents.

These results suggest that the dynamic capacity of the adsorbent bed with MOF-177 is higher than other sorbents. Reducing the dynamic mass transfer zone increases the dynamic capacity of the bed [100]. Higher values of k_1 , as for MOF-177, allow a steeper curve compared to others, suggesting that the bed is being utilized more efficiently [101].

Figure 3 also suggests that the bed with MIL-101 sorbent has a very low residence time (the time that the air has spent inside the adsorber), as also reported in the work of Sinha et al. [55] for a MIL-101-based sorbent.

Breakthrough curves for amine-based sorbents are shown in Figure 4.

The same three sections are present. However, a greater mass transfer zone is present for these chemisorbents compared the previous sorbents, due to a lower mass rate constant of $4 \times 10^{-4} \text{ s}^{-1}$ for the silica gel-based sorbent, and of $3.8 \times 10^{-3} \text{ s}^{-1}$ for the cellulose-based sorbent. In fact, the mass transfer zone for the SI-AEATPMS is around 14,380 s, while for APDES-NFC-FD it is 1915 s. A higher mass transfer resistance is present in chemisorbents. A steeper breakthrough curve in these last sorbents is due to a higher bed porosity, the effect of which is studied in the work of Papurello et al. [97]. However, even though chemisorbents are characterized by lower adsorption time constants, the breakthrough curve is shifted to later times, suggesting a stronger affinity between the adsorbent and CO_2 [102]. Since a chemical reaction occurs, a greater adsorption capacity is present, as shown in Figures 5 and 6, reporting, respectively, the trend of loading for physisorbents and chemisorbents as a function of time and length of adsorbent bed. The loading is defined as the adsorbed CO_2 and sorbent mass ratio, then it is depending on the adsorbent length.

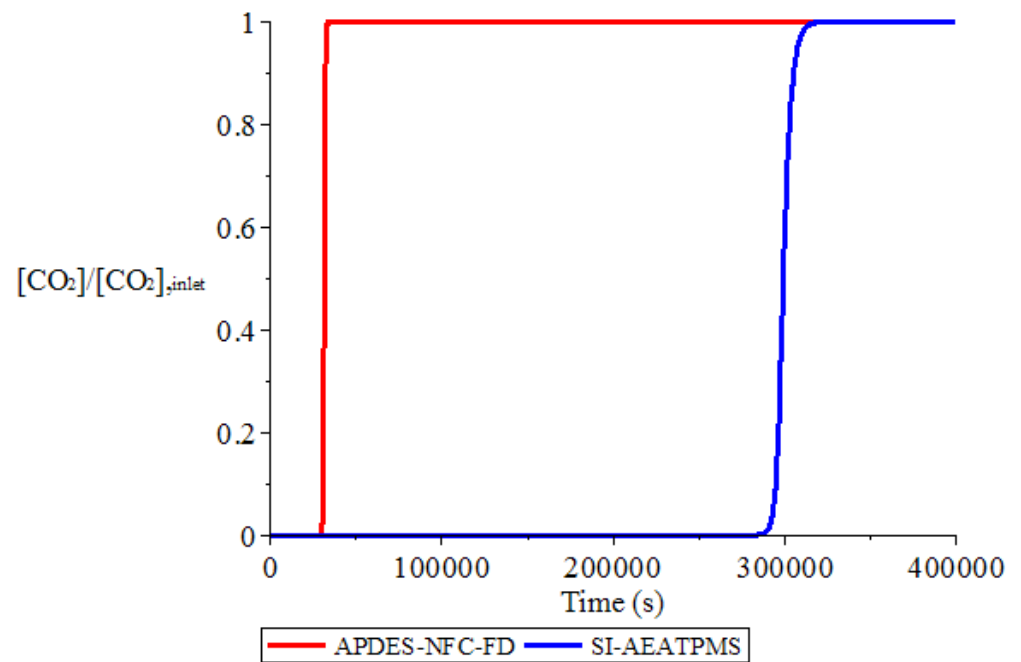


Figure 4. Breakthrough curves (CO_2 concentration at the outlet/ CO_2 concentration at the inlet) for chemisorbents.

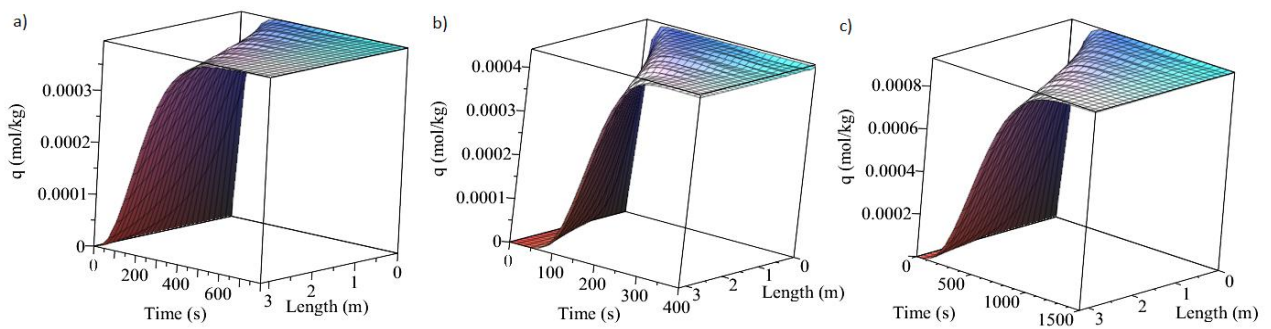


Figure 5. Loading for physisorbents: (a) MIL-101, (b) MOF-177, and (c) MOF-5.

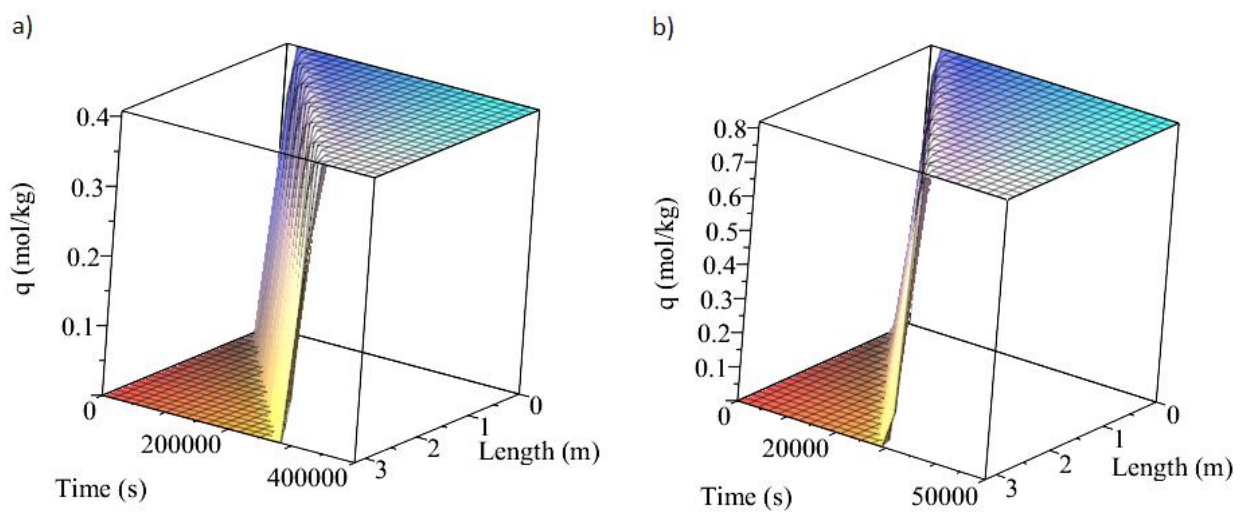


Figure 6. Loading for chemisorbents: (a) SI-AEATPMS sorbent and (b) APDES-NFC-FD sorbent.

Lower values of equilibrium loading are apparent for MOFs. For MOF-177, MOF-5, and MIL-101 this parameter is, respectively, 0.00043 mol/kg, 0.00093 mol/kg, and 0.00039 mol/kg. On the other hand, for SI-AEATPMS and APDES-NFC-FD the equilibrium loading is, respectively, 0.4 mol/kg and 0.85 mol/kg.

The above discussion is related to the adsorption stage, when CO₂ is captured by sorbent. Heating is provided for desorption, as in a TSA process. Figure 7 shows CO₂ concentration as a function of time and length for MOFs, while Figure 8 reports the same parameter for chemisorbents.

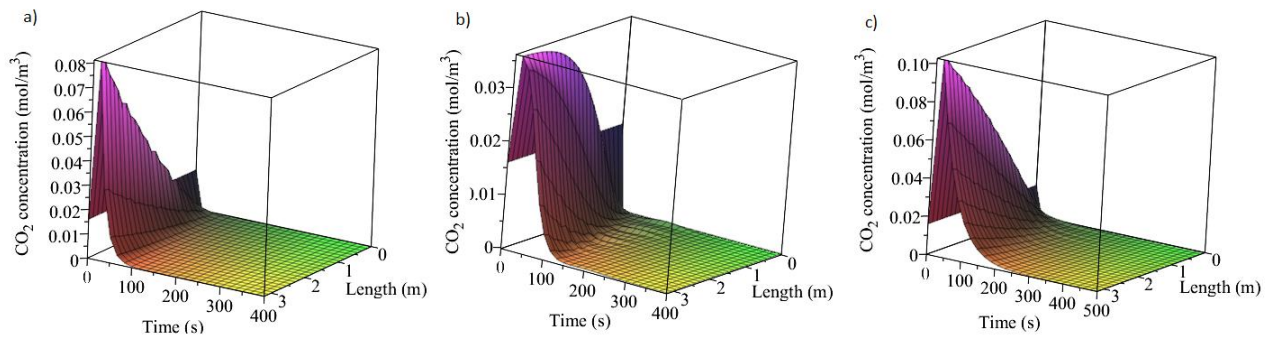


Figure 7. CO₂ concentration during the desorption step for physisorbents: (a) MIL-101, (b) MOF-177, and (c) MOF-5.

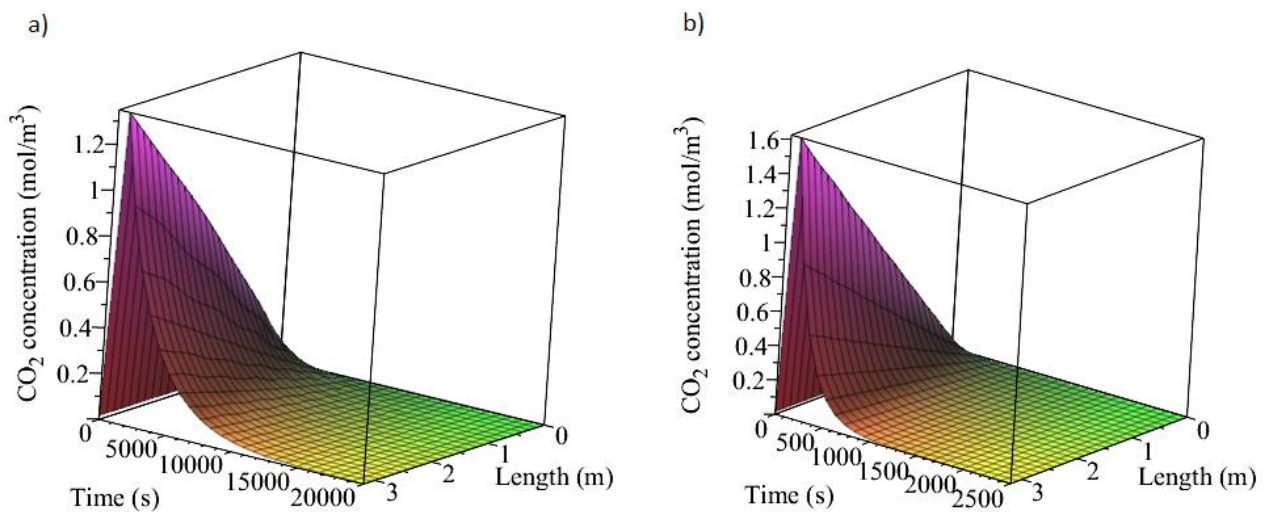


Figure 8. CO₂ concentration during the desorption step for chemisorbents: (a) SI-AEATPMS sorbent and (b) APDES-NFC-FD sorbent.

It is possible to see that the CO₂ concentration starts from a value corresponding to the inlet concentration of 0.016 mol/m³, has a maximum close to the inlet of bed and after that, it decreases towards zero, as also reported in the work of Morales–Ospino et al. [82]. The maximum value is due to the impact of heating when the bed is still saturated with CO₂. The loading starts from the value at the inlet condition and has a decreasing trend.

3.2. KPI: CO₂ Productivity of DAC Systems

From the previously discussed curves, related to the adsorption and desorption stages, it is possible to find adsorption and desorption times, the full cycle time, and then the CO₂ productivity (amount of CO₂ captured). The adsorption and desorption times are for a 90% approach to equilibrium and are in agreement with data reported in the literature [17,74].

The required mass of the sorbent is calculated knowing the volume and porosity of bed and particle density [103]. With all of this information, it is possible to evaluate the

average single pass recovery, R_c , and the amount of captured CO_2 . The average single pass recovery is defined as the ratio between the difference of CO_2 at the inlet and outlet of the bed and CO_2 at the inlet (in terms of mole). The adsorption time can also be calculated as the ratio between the 90% of equilibrium loading and mass sorbent product and the average single pass recovery and CO_2 mole in the feed product [104]. Then, the value of R_c can be obtained by iteration to a self-consistent value.

The full cycle time (including adsorption and desorption times), average single pass recovery, the mass of the sorbent, and captured CO_2 are evaluated for each sorbent as reported in Table 10.

Table 10. Main results from adsorption and desorption stages.

Sorbent	MIL-101	MOF-177	MOF-5	SI-AEATPMS	APDES-NFC-FD
Mass of the sorbent (kg)	2.22×10^4	1.54×10^4	2.23×10^4	3.36×10^4	1.77×10^3
Average single pass recovery	5.2×10^{-1}	5.9×10^{-1}	5.3×10^{-1}	8.6×10^{-1}	8.9×10^{-1}
Adsorption time (s)	3.2×10^2	2.14×10^2	7.49×10^2	3.06×10^5	3.26×10^4
Desorption time (s)	9.9×10^1	1.6×10^2	3.15×10^2	1.67×10^4	1.85×10^3
Full cycle time (h)	1.2×10^{-1}	9×10^{-2}	2.9×10^{-1}	8.92×10^1	9.53
Number of cycles/day	2.07×10^2	2.71×10^2	8.15×10^1	3×10^{-1}	2.5
Captured CO_2 (kg/h)	3.96	4.5	4.00	6.43	6.66
Captured CO_2 (kg/cycle)	3.5×10^{-1}	2.6×10^{-1}	8.3×10^{-1}	546×10^2	6.03×10^1
Captured CO_2 (kg/day)	7.3×10^1	7.2×10^1	6.8×10^1	1.47×10^2	1.52×10^2

Due to a higher adsorption capacity, as discussed above, chemisorbents are able to capture a greater amount of CO_2 : 6.43 kgCO_2/h and 6.66 kgCO_2/h , respectively, for the silica gel-based sorbent and the cellulose-based sorbent, compared to physisorbents. The MOFs MIL-101, MOF-177, and MOF-5 capture, respectively, 3.96 $\text{kg CO}_2/\text{h}$, 4.5 kgCO_2/h , and 4 kgCO_2/h . The best performances of MOF-177 and APDES-NFC-FD among the physisorbents and chemisorbents are due to a lower mass transfer zone, and are underlined by a greater amount of captured CO_2 , and then by a higher value of the average single pass recovery, which is 0.89 for the cellulose-based sorbent and 0.59 for MOF-177.

Adsorption and desorption times are higher for amine-functionalized sorbents. Additionally, the higher value for the SI-AEATPMS sorbent compared to the other amine-based sorbent is due to the higher amine content of the APDES-NFC-FD sorbent [105]. In fact, results show that a full cycle for the silica gel-based sorbent is 89.2 h (305,500 s for the adsorption time and 16,650 for the desorption time), while only 9.53 h (32,560 s for the adsorption time and 1845 s for the desorption time) are required for the cellulose-based sorbent. For MOFs, full cycle times are lower than 1 h: the lowest value is for MOF-177 for which this parameter is 0.09 h (214 s for the adsorption time and 106 s for the desorption time). For this reason, the number of cycles per day is higher using physisorbent: MOF-177 conducts 271 cycles/day, while 0.3 cycles/day are needed for SI-AEATPMS sorbent.

Overall, amine-functionalized sorbents capture 152 kgCO_2/day (APDES-NFC-FD sorbent) and 147 kgCO_2/day (SI-AEATPMS), while MIL-101, MOF-177, and MOF-5 capture, respectively, 73 kgCO_2/day , 72 kgCO_2/day , and 68 kgCO_2/day .

3.3. KPIs: Energy Consumption and Cost of DAC Systems

As explained previously, energy consumption includes the electrical energy for fans blowing air inside the bed, and thermal energy for the regeneration. Table 11 shows the amount of energy required for each sorbent.

It is possible to underline why physisorbents are characterized by higher values of energy consumption in terms of both electrical and thermal energy. The electrical energy demand is higher for MOFs due to higher pressure drop and lower amount of captured CO_2 per day, compared to systems using amine-functionalized sorbents. The required electricity energy for MOFs and amine-functionalized sorbents is comparable with the values reported by Fasihi et al. [53] in their work. In our research, the electricity con-

sumption for MIL-101, MOF-177, and MOF-5 are, respectively, 1540 kWh_{el}/tonneCO₂, 1350 kWh_{el}/tonneCO₂, and 1520 kWh_{el}/tonneCO₂. The amine-based sorbents exhibit lower values: 357 kWh_{el}/tonneCO₂ and 299 kWh_{el}/tonneCO₂, respectively, for SI-AEATPMS and APDES-NFC-FD.

Table 11. Energy consumptions for different adsorbent beds.

Sorbent	MIL-101	MOF-177	MOF-5	SI-AEATPMS	APDES-NFC-FD
Regeneration mode	TSA	TSA	TSA	TSA	TSA
Regeneration temperature (K)	3.73×10^2	3.73×10^2	3.73×10^2	3.83×10^2	3.73×10^2
Pressure drop (Pa)	1.94×10^3	1.94×10^3	1.94×10^3	7.34×10^2	6.36×10^2
Electrical energy (kWh _{el} /tonneCO ₂)	1.54×10^3	1.35×10^3	1.52×10^3	3.57×10^2	2.99×10^2
Working capacity (mol/kg)	3.5×10^{-4}	3.9×10^{-4}	8.4×10^{-4}	3.67×10^{-1}	7.71×10^{-1}
Regeneration energy (kWh _{th} /tonneCO ₂)	1.07×10^6	1.3×10^6	4.94×10^5	1.88×10^3	1.4×10^3

Particular consideration is required for the thermal energy to regenerate the sorbent. No data of this parameter are present for MOFs capturing CO₂ from air in the literature.

For amine-functionalized sorbents, values similar to those reported by Fasihi et al. [53], Elfving et al. [106], and Wijesiri et al. [3] are obtained: 1884 kWh_{th}/tonneCO₂ for the silica gel-based sorbent and 1427 kWh_{th}/tonneCO₂ for the cellulose-based sorbent.

However, higher values are obtained for physisorbents, ranging from 494,000 kWh_{th}/tonneCO₂ for MOF-5 to 1,300,000 for MOF-177 (due to the sensible heating requirements for the sorbent). These greater values are due to a very low working capacity for MOFs, ranging from 0.00084 mol/kg for MOF-5 to 0.00035 mol/kg for MIL-101 under atmospheric concentration of CO₂. Working capacity depends on the equilibrium loading, this is then a critical parameter for the design of adsorption processes. This is an important finding in the context of MOFs.

Moreover, it is evident that DAC facilities using MOFs are impracticable due the huge amount of thermal energy requirement. This is true not only for an energetic point of view but also for an environmental aspect because additional CO₂ would be emitted by the MWI to produce the heat energy needed to regenerate the adsorbent.

For DAC processes based on amine-functionalized sorbents, a life cycle assessment analysis is suggested to account for the additional emissions of MWI.

Economic analysis is carried out with the evaluation of CAPEX and OPEX for each process with different sorbents. Table S3 shows the analysis of capital costs for different adsorbent beds, starting from the evaluation of equipment (adsorber and fan) costs. For the adsorber, the mass of the shell of carbon steel is calculated according to the relation provided by Towler and Sinnott [107] and equal to 1200 kg. For the fan, the impeller diameter is evaluated to be 0.38 m [108]. Overall, CAPEX is determined by the sum of working capital and fixed capital investment, working capital assumed to be 15% of total capital investment.

Results show that for all sorbents, annualized capital costs are 11500 USD/year, while the CAPEX cost breakdown is reported in Figure S2. Specific capital costs are lower for amine-functionalized sorbents: 214 USD/tonneCO₂ for the cellulose-based sorbent and 221 USD/tonneCO₂ for the silica gel-based sorbent. For MIL-101, MOF-177, and MOF-5, specific capital costs are, respectively, 446 USD/tonneCO₂, 447 USD/tonneCO₂, and 479 USD/tonneCO₂.

The evaluation of operating costs is reported in Table S4 while the OPEX breakdown cost is reported in Figures S3–S7. Here, the OPEX is different for each adsorbent bed, and higher operating costs are required for physisorbents due to higher costs for utilities, especially cooling water (since a greater amount of cooling water is required to remove the greater overall amount of heat that is required for the regeneration step) and thermal energy. Specific OPEX for SI-AEATPMS and APDES-NFC-FD are, respectively 7.756 USD/tonneCO₂ and 5.537 USD/tonneCO₂. On the other hand, for MIL-101,

MOF-177, and MOF-5 these costs are 66,100 USD/tonneCO₂, 38,900 USD/tonneCO₂, and 15,800 USD/tonneCO₂.

Overall, total costs are 751 USD/tonneCO₂ for the cellulose-based sorbent, 977 USD/tonneCO₂ for the silica gel-based sorbent, 66,600 USD/tonneCO₂ for the MIL-101 sorbent, 39,400 USD/tonneCO₂ for the MOF-177 sorbent, and 16,300 USD/tonneCO₂ for the MOF-5 sorbent.

The economic analysis suggests that operating costs have the highest influence on total costs for all investigated systems, especially for those using MOFs.

In particular, the contribution of OPEX and CAPEX on total costs is, respectively, 72% and 28% for the system using the cellulose-based sorbent, 77% and 23% for the system using the silica gel-based sorbent, 99% and 1% for the process using MIL-101 and MOF-177, and 97% and 3% for the system using MOF-5.

For the capture system using the SI-AEATPMS sorbent, the cost of cooling water is significant, suggesting the use of free air for the cooling stage in order to reduce costs. Another significant contribution is from the maintenance and repairs cost, which is evaluated as 2% of the fixed capital investment. This cost could be reduced by using equipment with another material that with a lower carbon content could allow lower costs.

For the capture system using the APDES-NFC-FD sorbent, the maintenance and repair cost is the most significant element OPEX; hence, the use of another material for equipment could help in cost reduction. The cooling water cost has a great influence on OPEX too.

Overall, for processes using amine-functionalized sorbents, it is suggested to use alternative materials of construction and use free air for cooling.

For capture systems based on MOF-5 and MOF-177, the cost for the required thermal energy is the most significant, while for the process capturing CO₂ using MIL-101 the cost of cooling water has the highest contribution, although the cost of thermal energy is great too. This suggests that a reduction in costs could be achieved by using air as a cooling medium (as already done in the Antecy Company) and improving the sorbent efficiency of MOFs in terms of loading, which is a critical parameter, as mentioned before. Future research should be focused on improving the efficiency of these new materials, still under study and characterized by unprecedented chemical and structural tunability.

Moreover, from the economic analysis we found that the lowest total cost is for the process using the chemisorbent APDES-NFC-FD, while the highest cost is for the process using the physisorbent MIL-101.

According to the previous considerations (OPEX with the highest influence on total costs with direct production costs as the main contribution as in Figures S4–S7), we can say that the total costs can range according to the price of significant utilities and raw materials in the market, for the capture system using the silica gel-based sorbent and MOFs.

For the process based on the cellulose sorbent, fixed charges have the highest influence on OPEX so we expect that total costs can range $\pm 20\%$.

In any case, total costs for amine-based sorbents are in agreement with the order of magnitude estimated by House et al. [109] for DAC systems up to 1000 \$/tonCO₂.

The consideration is for other costs reported in the literature and revised by the work of Fasihi et al. [53]. These reported costs are of a few hundred dollars per tonne of CO₂ and are based on different assumptions [3,98]. In particular, a few hundred dollars per tonne of captured CO₂ are estimated by Kulkarni and Sholl [54], Zhang et al. [18], and Sinha et al. [55]. However, Krekel et al. [110] report in their work that once capital costs are considered, the total capture cost increases significantly.

Particular attention should be placed on the use of MOFs, since due to higher operating costs caused by the very low working capacity, these are very expensive for CO₂ capture from air and are not recommended. Future research should be focused on the development of MOFs that ensure higher values of loading. This could be achieved by adding special compounds. This solution could make MOFs suitable for CO₂ capture.

3.4. Comparison with Climeworks Data

Climeworks has developed a DAC plant at semi-commercial scale, and uses an amine-functionalized cellulose chemisorbent, as discussed here. The geometry of the adsorbent bed is the same as that used in our calculation. Overall, results show a good agreement between operating conditions and energy consumptions evaluated by us for the APDES-NFC-FD sorbent with those reported proposed by this DAC Company.

The duration of a full cycle is lower for Climeworks and in the range of 4–6 h, because only the adsorption of CO₂ is considered in our model, whereas some humidity is present in the real air flow rate. However, experimental analyses show that after 5 h adsorption time, the CO₂ uptake curves are still on an upwards path, while the corresponding H₂O curves have reached a steady state for all relative humidity values [105]. This explains why Climeworks utilizes a shorter cycle.

For other operating parameters, no significant differences are present. In fact, for Climeworks the amount of captured CO₂ is 135 kgCO₂/day, with an average single pass recovery of 0.9. Regarding the energetic consumption, the proposed electrical energy consumption is between 200 kWh_{el}/tonneCO₂ and 450 kWh_{el}/tonneCO₂. The required thermal energy consumption is 1500–2000 kWh_{th}/tonneCO₂.

Regarding the economic analysis, our total cost (751 USD/tonneCO₂) is the same order of magnitude of that proposed by Climework (600 USD/tonneCO₂) [111].

Moreover, our calculated total cost can be higher than that estimated when humidity is present in the air. In fact, as reported in Wurzbacher et al. [104], the energy consumption for the regeneration can increase up to 20% when the relative humidity increases from 20% to 80%.

4. Conclusions

An independent analysis is developed in this research work to evaluate some KPIs (energy consumption, CO₂ productivity, and costs) of a DAC processes, based on adsorption using different sorbents. In particular, chemisorbents (two amine-functionalized sorbents, SI-AEATPMS and APDES-NFC-FD) and physisorbents (three MOFs: MIL-101, MOF-5, and MOF-177) are compared.

For this purpose, a mathematical model describing adsorption and desorption stages is developed for each sorbent.

Results show that MOFs are characterized by a very low equilibrium loading and hence a very low working capacity in comparison to chemisorbents. For MIL-101, MOF-177, and MOF-5 this last parameter is, respectively, 0.00035 mol/kg, 0.00039 mol/kg, and 0.00084 mol/kg. On the other hand, for SI-AEATPMS and APDES-NFC-FD working capacity is, respectively, 0.367 mol/kg and 0.771 mol/kg.

The equilibrium loading is a critical parameter because it influences the adsorption capacity, energy consumption, and cost. Better results are found for the adsorption processes using amine-functionalized sorbents. For the cellulose-based sorbent, 152 kgCO₂/day are captured, consuming 299 kWh_{el}/tonneCO₂ of electrical energy and 1427 kWh_{th}/tonneCO₂ of thermal energy at an overall total cost of 751 USD/tonneCO₂. For MOF-177, the amount of captured CO₂, electrical energy and thermal energy consumptions, and total costs are, respectively, 72 kgCO₂/day, 1350 kWh_{el}/tonCO₂, 1,300,000 kWh_{th}/tonCO₂, and 39,400 USD/tonneCO₂. It is evident that the huge amount of thermal energy requirement makes the processes based on MOFs impracticable.

This independent analysis shows that costs reported in the literature appear to be with the same order of magnitude of our analysis. A comparison with the Climeworks Company (using the APDES-NFC-FD sorbent) shows a good agreement with KPIs, and total cost. Higher costs are expected when humidity is in the air.

It is important to note that we are assuming here the availability of industrial waste heat—should this not be available, costs will be somewhat higher (22%, when a traditional boiler is used for heating, considering a cost for heat of 0.165 USD/kWh [112]). Suggestions to reduce costs are provided. It was found that for systems using amine-functionalized

sorbents, the use of air for the cooling stage and cheaper materials for equipment could reduce OPEX and therefore overall costs. For processes using MOFs, more research should be focused to improve their loading allowing a lower cost for thermal energy. The use of air for cooling could reduce costs too.

Supplementary Materials: The following supporting information can be downloaded at: <https://www.mdpi.com/article/10.3390/app12052618/s1>, Figure S1: Breakthrough curve (CO₂ concentration at the outlet/CO₂ concentration at the inlet) for the experimental apparatus used in Wurzbacher (2015); Figure S2: Breakdown of the main contributions (cut-off 5%) to CAPEX for all adsorbent beds; Figure S3: Breakdown of the main contributions (cut-off 5%) to OPEX for the adsorbent beds with APDES-NFC-FD; Figure S4: Breakdown of the main contributions (cut-off 5%) to OPEX for the adsorbent beds with SI-AEATPMS; Figure S5: Breakdown of the main contributions (cut-off 5%) to OPEX for the adsorbent beds with MIL-101; Figure S6: Breakdown of the main contributions (cut-off 5%) to OPEX for the adsorbent beds with MOF-177; Figure S7: Breakdown of the main contributions (cut-off 5%) to OPEX for the adsorbent beds with MOF-5. Table S1: Dimensionless number values of the mathematical model; Table S2: Inputs used in Matches calculator for cost analysis; Table S3: CAPEX of different adsorbent beds; Table S4: OPEX of different adsorbent beds.

Author Contributions: Conceptualization, P.S.F., G.L. and N.S.; methodology, G.L. and N.S.; formal analysis, G.L.; investigation, G.L.; writing—original draft preparation, G.L.; writing—review and editing, P.S.F. and N.S.; supervision, P.S.F. and N.S.; funding acquisition, P.S.F. and N.S. All authors have read and agreed to the published version of the manuscript.

Funding: This research was funded by the Hadley Trust.

Institutional Review Board Statement: Not applicable.

Informed Consent Statement: Not applicable.

Data Availability Statement: UKCCSRC data repository.

Acknowledgments: This work was supported by the Hadley Trust.

Conflicts of Interest: The authors declare no conflict of interest.

References

- IEA. 2020. Available online: <https://www.iea.org/data-and-statistics/?country=WORLD&fuel=CO2%20emissions&indicator=TotCO2> (accessed on 1 November 2020).
- Bui, M.; Adjiman, C.S.; Bardow, A.; Boston, A.; Brown, S.; Fennell, P.S.; Fuss, S.; Galindo, A.; Hackett, L.A.; et al. Carbon capture and storage (CCS): The way forward. *Energy Environ. Sci.* **2018**, *11*, 1062–1176. [[CrossRef](#)]
- Wijesiri, R.P.; Knowles, G.P.; Yeasmin, H.; Hoadley, A.F.A.; Chaffee, A.L. Technoeconomic Evaluation of a Process Capturing CO₂ Directly from Air. *Processes* **2019**, *7*, 503. [[CrossRef](#)]
- Sanz-Pérez, E.; Murdock, C.R.; Didas, S.A.; Jones, C.W. Direct Capture of CO₂ from Ambient Air. *Chem. Rev.* **2016**, *116*, 11840–11876. [[CrossRef](#)]
- Zhu, X.; Ge, T.; Yang, F.; Wang, R. Design of steam-assisted temperature vacuum-swing adsorption processes for efficient CO₂ capture from ambient air. *Renew. Sustain. Energy Rev.* **2020**, *137*, 110651. [[CrossRef](#)]
- Lackner, K.S.; Ziock, H.J.; Grimes, P. *Carbon Dioxide Extraction from Air: Is It an Option?* Los Alamos National Lab.: Los Alamos, NM, USA, 1999.
- Fuss, S.; Lamb, W.F.; Callaghan, M.W.; Hilaire, J.; Creutzig, F.; Amann, T.; Beringer, T.; de Oliveira Garcia, W.; Hartmann, J.; Khanna, T.; et al. Negative emissions—Part 2: Costs, potentials and side effects, *Environ. Res. Lett.* **2018**, *13*, 063002. [[CrossRef](#)]
- Kar, S.; Sen, R.; Goepfert, A.; Prakash, G.K.S. Integrative CO₂ Capture and Hydrogenation to Methanol with Reusable Catalyst and Amine: Toward a Carbon Neutral Methanol Economy. *J. Am. Chem. Soc.* **2018**, *140*, 1580–1583. [[CrossRef](#)]
- Bos, M.J.; Kersten, S.R.A.; Brilman, D.W.F. Wind power to methanol: Renewable methanol production using electricity, electrolysis of water and CO₂ air capture. *Appl. Energy* **2020**, *264*, 114672. [[CrossRef](#)]
- Shi, X.; Xiao, H.; Azarabadi, H.; Song, J.; Wu, X.; Chen, X.; Lackner, K.S. Sorbents for the Direct Capture of CO₂ from Ambient Air. *Angew. Chem. Int. Ed.* **2020**, *59*, 6984–7006. [[CrossRef](#)]
- Sabatino, F.; Mehta, M.; Grimm, A.; Gazzani, M.; Gallucci, F.; Kramer, G.J.; Annaland, M.V.S. Evaluation of a Direct Air Capture Process Combining Wet Scrubbing and Bipolar Membrane Electrodialysis. *Ind. Eng. Chem. Res.* **2020**, *59*, 7007–7020. [[CrossRef](#)]
- Eisaman, M.D.; Schwartz, D.E.; Amic, S.; Larnier, D.L.; Zesch, J.; Torres, F.; Littau, K. Energy-Efficient Electrochemical CO₂ Capture from the Atmosphere. In Proceedings of the 2009 Clean Technology Conference and Trade Show, Houston, TX, USA, 3–7 May 2009.

13. Kelemen, P.B.; McQueen NWilcox, J.; Renforth, P.; Dipple, G.; Vankeuren, A.P. Engineered carbon mineralization in ultramafic rocks for CO₂ removal from air: Review and new insights. *Chem. Geol.* **2020**, *550*, 119628. [CrossRef]
14. von Hippel, T. Thermal Removal of Carbon Dioxide from the Atmosphere: Energy Requirements and Scaling Issues. *Clim. Change* **2018**, *148*, 491–501. [CrossRef]
15. Adamu, A.; Abegão, F.R.; Boodhoo, K. Process intensification technologies for CO₂ capture and conversion—A review. *BMC Chem. Eng.* **2020**, *2*, 2. [CrossRef]
16. Realmonte, G. Direct Air Capture and Negative Emission Technologies in Deep Mitigation Pathways. Master's Thesis, Politecnico of Milano, Milan, Italy, 2017.
17. Qasem, N.A.A.; Ben-Mansour, R. Adsorption breakthrough and cycling stability of carbon dioxide separation from CO₂/N₂/H₂O mixture under ambient conditions using 13X and Mg-MOF-74. *Appl. Energy* **2018**, *230*, 1093–1107. [CrossRef]
18. Zhang, W.; Liu, H.; Sun, C.; Drage, T.C.; Snape, C.E. Capturing CO₂ from ambient air using a polyethyleneimine–silica adsorbent in fluidized beds. *Chem. Eng. Sci.* **2014**, *116*, 306–316. [CrossRef]
19. Shekhah, O.; Belmabkhout, Y.; Chen, Z.; Guillerm, V.; Cairns, A.; Adil, K.; Eddaoudi, M. Made-to-order metal-organic frameworks for trace carbon dioxide removal and air capture. *Nat. Commun.* **2014**, *5*, 4228. [CrossRef]
20. Bahamon, D.; Díaz-Márquez Pablo Gamallo, A.; Vega, L.F. Energetic evaluation of swing adsorption processes for CO₂ capture in selected MOFs and zeolites: Effect of impurities. *Chem. Eng. J.* **2018**, *342*, 458–473. [CrossRef]
21. Li, J.-R.; Ma, Y.; McCarthy, M.C.; Sculley, J.; Yu, J.; Jeong, H.-K.; Balbuena, P.B.; Zhou, H.-C. Carbon dioxide capture-related gas adsorption and separation in metal-organic frameworks. *Coord. Chem. Rev.* **2011**, *255*, 1791–1823. [CrossRef]
22. Li, J.R.; Sculley, J.; Zhou, H.C. Metal-organic frameworks for separations. *Chem. Rev.* **2012**, *112*, 869–932. [CrossRef]
23. Gaikwad, S.; Kim, Y.; Han, S. Enhanced CO₂ capture capacity of amine-functionalized MOF-177 metal organic framework. *J. Environ. Chem. Eng.* **2021**, *9*, 105523. [CrossRef]
24. Demir, H.; Keskin, S. Hypothetical yet Effective: Computational Identification of High-performing MOFs for CO₂ Capture. *Comput. Chem. Eng.* **2022**, *55*, 101811. [CrossRef]
25. Al-Rowaili, F.N.; Zahid, U.; Onaizi, S.; Khaled, M.; Jamal, A.; Al-Mutairi, E.M. A review for Metal-Organic Frameworks (MOFs) utilization in capture and conversion of carbon dioxide into valuable products. *J. CO₂ Util.* **2021**, *53*, 101715. [CrossRef]
26. Gaikwad, S.; Kim, S.-J.; Han, S. CO₂ capture using amine-functionalized bimetallic MIL-101 MOFs and their stability on exposure to humid air and acid gases. *Microporous Mesoporous Mater.* **2018**, *277*, 253–260. [CrossRef]
27. Ben-Mansour, R.; Qasem, N.A.A.; Antar, M.A. Carbon dioxide adsorption separation from dry and humid CO₂/N₂ mixture. *Comput. Chem. Eng.* **2018**, *117*, 221–235. [CrossRef]
28. NovoMOF. 2021. Available online: <https://blog.novomof.com/blog/gas-separation-zeolites-vs-mofs> (accessed on 1 March 2021).
29. Yu, J.; Chuang, S.S.C. The Role of Water in CO₂ Capture by Amine. *Ind. Eng. Chem. Res.* **2017**, *56*, 6337–6347. [CrossRef]
30. Belmabkhout, Y.; Serna-Guerrero, R.; Sayari, A. Amine-bearing mesoporous silica for CO₂ removal from dry and humid air. *Chem. Eng. Sci.* **2010**, *65*, 3695–3698. [CrossRef]
31. Goepfert, A.; Zhang, H.; Czaun, M.; May, R.B.; Prakash, G.K.S.; Olah, G.A.; Narayanan, S.R. Easily Regenerable Solid Adsorbents Based on Polyamines for Carbon Dioxide Capture from the Air. *ChemSusChem* **2014**, *7*, 1386–1397. [CrossRef] [PubMed]
32. Kwon, H.T.; Sakwa-Novak, M.A.; Pang, S.; Sujana, A.R.; Ping, E.W.; Jones, C.W. Aminopolymer-Impregnated Hierarchical Silica Structures: Unexpected Equivalent CO₂ Uptake under Simulated Air Capture and Flue Gas Capture Conditions. *Chem. Mater.* **2019**, *31*, 5229–5237. [CrossRef]
33. Sarazen, M.L.; Sakwa-Novak, M.A.; Ping, E.W.; Jones, C.W. Effect of different acid initiators on branched poly(propyleneimine) synthesis and CO₂ sorption performance. *ACS Sustain. Chem. Eng.* **2019**, *7*, 7338–7345. [CrossRef]
34. Wagner, A.; Steen, B.; Johansson, G.; Zanghellini, E.; Jacobsson, P.; Johansson, P. Ran Carbon Dioxide Capture from Ambient Air Using Amine-Grafted Mesoporous Adsorbents. *Int. J. Spectrosc.* **2013**, *2013*, 690186. [CrossRef]
35. Potter, M.E.; Cho, K.M.; Lee, J.J.; Jones, C.W. Role of Alumina Basicity in CO₂ Uptake in 3-Aminopropylsilyl-Grafted Alumina Adsorbents. *ChemSusChem* **2017**, *10*, 2192–2201. [CrossRef] [PubMed]
36. Abhilash, K.A.S.; Deepthi, T.; Sadhana, R.A.; Benny, K.G. Functionalized Polysilsesquioxane-Based Hybrid Silica Solid Amine Sorbents for the Regenerative Removal of CO₂ from Air. *ACS Appl. Mater. Interfaces* **2015**, *7*, 17969–17976. [CrossRef] [PubMed]
37. Lee, W.R.; Hwang, S.Y.; Ryu, D.W.; Lim, K.S.; Han, S.S.; Moon, D.; Choi, J.; Hong, C.S. Diamine-Functionalized Metal–organic Framework: Exceptionally High CO₂ Capacities from Ambient Air and Flue Gas, Ultrafast CO₂ Uptake Rate, and Adsorption Mechanism. *Energy Environ. Sci.* **2014**, *7*, 744–751. [CrossRef]
38. McDonald, T.M.; Lee, W.R.; Mason, J.A.; Wiers, B.M.; Hong, C.S.; Long, J.R. Capture of Carbon Dioxide from Air and Flue Gas in the Alkylamine-Appended Metal–Organic Framework mmen-Mg₂(dobpdc). *J. Am. Chem. Soc.* **2012**, *134*, 7056–7065. [CrossRef] [PubMed]
39. Kumar, A.; Madden, D.G.; Lusi, M.; Chen, K.-J.; Daniels, E.A.; Curtin, T.; Perry, J.J.; Zaworotko, M.J. Direct Air Capture of CO₂ by Physisorbent Materials. *Angew. Chem. Int. Ed.* **2015**, *54*, 14372–14377. [CrossRef]
40. Choi, S.; Watanabe, T.; Bae, T.-H.; Sholl, D.S.; Jones, C.W. Modification of the Mg/DOBDC MOF with Amines to Enhance CO₂ Adsorption from Ultradilute Gases. *J. Phys. Chem. Lett.* **2012**, *3*, 1136–1141. [CrossRef] [PubMed]
41. Pirngruber, G.D.; Hamon, L.; Bourrelly, S.; Llewellyn, P.L.; Lenoir, E.; Guillerm, V.; Serre, C.; Devic, T. A Method for Screening the Potential of MOFs as CO₂ Adsorbents in Pressure Swing Adsorption Processes. *ChemSusChem* **2012**, *5*, 762–776. [CrossRef] [PubMed]

42. Meth, S.; Goeppert, A.; Prakash, G.K.S.; Olah, G.A. Silica Nanoparticles as Supports for Regenerable CO₂ Sorbents. *Energy Fuels* **2012**, *26*, 3082–3090. [CrossRef]
43. Brilman, D.W.F.; Veneman, R. Capturing atmospheric CO₂ using supported amine sorbents. *Energy Procedia* **2013**, *37*, 6070–6078. [CrossRef]
44. Pang, S.H.; Jue, M.L.; Leisen, J.; Jones, C.W.; Lively, R.P. PIM-1 as a solution-processable “molecular basket” for CO₂ capture from dilute sources. *ACS Macro Lett.* **2015**, *4*, 1415–1419. [CrossRef]
45. Chaikittisilp, W.; Khunsupat, R.; Chen, T.T.; Jones, C.W. Poly(allylamine)–Mesoporous Silica Composite Materials for CO₂ Capture from Simulated Flue Gas or Ambient Air. *Ind. Eng. Chem. Res.* **2011**, *50*, 14203–14210. [CrossRef]
46. Gebald, C.; Wurzbacher, J.A.; Borgschulte, A.; Zimmermann, T.; Steinfeld, A. Single-Component and Binary CO₂ and H₂O Adsorption of Amine-Functionalized Cellulose. *Environ. Sci. Technol.* **2014**, *48*, 2497–2504. [CrossRef]
47. Liao, P.-Q.; Chen, X.-W.; Liu, S.-Y.; Li, X.-Y.; Xu, Y.-T.; Tang, M.; Rui, Z.; Ji, H.; Zhang, J.-P.; Chen, X.-M. Putting an ultrahigh concentration of amine groups into a metal–organic framework for CO₂ capture at low pressures. *Chem. Sci.* **2016**, *7*, 6528–6533. [CrossRef] [PubMed]
48. Ng, Y.C.; Yang, L.; Jovanovic, Z.R. The Development and Validation of a Closed-Loop Experimental Setup for Investigating CO₂ and H₂O Coadsorption Kinetics under Conditions Relevant to Direct Air Capture. *Ind. Eng. Chem. Res.* **2018**, *57*, 13987–13998. [CrossRef]
49. Choi, S.; Drese, J.H.; Eisenberger, P.M.; Jones, C.W. Application of Amine-Tethered Solid Sorbents for Direct CO₂ Capture from the Ambient Air. *Environ. Sci. Technol.* **2011**, *45*, 2420–2427. [CrossRef]
50. Shekhah, O.; Belmabkhout, Y.; Adil, K.; Bhatt, P.M.; Cairns, A.J.; Eddaoudi, M. A facile solvent-free synthesis route for the assembly of a highly CO₂ selective and H₂S tolerant NiSIFSIX metal–organic framework. *Chem. Commun.* **2015**, *51*, 13595–13598. [CrossRef] [PubMed]
51. Caskey, S.R.; Wong-Foy, A.G.; Matzger, A.J. Dramatic Tuning of Carbon Dioxide Uptake via Metal Substitution in a Coordination Polymer with Cylindrical Pores. *J. Am. Chem. Soc.* **2008**, *130*, 10870–10871. [CrossRef]
52. Al-Janabi, N.; Vakili, R.; Kalumpasut, P.; Gorgojo, P.; Siperstein, F.R.; Fan, X.; McCloskey, P. Velocity variation effect in fixed bed columns: A case study of CO₂ capture using porous solid adsorbents. *AIChE J.* **2018**, *64*, 2189–2197. [CrossRef]
53. Fasihi, M.; Efimova, O.; Breyer, C. Techno-economic assessment of CO₂ direct air capture plants. *J. Clean. Prod.* **2019**, *224*, 957–980. [CrossRef]
54. Kulkarni, A.R.; Sholl, D.S. Analysis of Equilibrium-Based TSA Processes for Direct Capture of CO₂ from Air. *Ind. Eng. Chem. Res.* **2012**, *51*, 8631–8645. [CrossRef]
55. Sinha, A.; Darunte, L.A.; Jones, C.W.; Realff, M.J.; Kawajiri, Y. Systems Design and Economic Analysis of Direct Air Capture of CO₂ through Temperature Vacuum Swing Adsorption Using MIL-101(Cr)-PEI-800 and mmen-Mg₂(dobpdc) MOF Adsorbents. *Ind. Eng. Chem. Res.* **2017**, *56*, 750–764. [CrossRef]
56. Viebahn, P.; Scholz, A.; Zelt, O. The Potential Role of Direct Air Capture in the German Energy Research Program—Results of a Multi-Dimensional Analysis. *Energies* **2019**, *12*, 3443. [CrossRef]
57. Kintisch, E. Can Sucking CO₂ Out of the Atmosphere Really Work? 2019. Available online: <https://www.technologyreview.com/s/531346/can-sucking-co2-out-of-the-atmosphere-really-work/> (accessed on 25 July 2019).
58. Sabatino, F.; Grimm, A.; Gallucci, F.; van Sint Annaland, M.; Kramer, G.J.; Gazzani, M. A comparative energy and costs assessment and optimization for direct air capture technologies. *Joule* **2021**, *in press*.
59. Schellevis, H.; van Schagen, T.; Brilman, D. Process optimization of a fixed bed reactor system for direct air capture. *Int. J. Greenh. Gas Control* **2021**, *110*, 103431. [CrossRef]
60. Miao, Y.; He, Z.; Zhu, X.; Izikowitz, D.; Li, J. Operating temperatures affect direct air capture of CO₂ in polyamine-loaded mesoporous silica. *Chem. Eng. J.* **2021**, *426*, 131875. [CrossRef]
61. van Schagen, T.; van der Wal, P.; Brilman, D. Development of a novel, through-flow microwave-based regenerator for sorbent-based direct air capture. *Chem. Eng. J. Adv.* **2021**, *9*, 100187. [CrossRef]
62. Drechsler, C.; Agar, D.W. Simulation and optimization of a novel moving belt adsorber concept for the direct air capture of carbon dioxide. *Comput. Chem. Eng.* **2019**, *126*, 520–534. [CrossRef]
63. Zhao, R.; Liu, L.; Zhao, L.; Deng, S.; Li, S.; Zhang, Y.; Li, H. Thermodynamic exploration of temperature vacuum swing adsorption for direct air capture of carbon dioxide in buildings. *Energy Convers. Manag.* **2019**, *183*, 418–426. [CrossRef]
64. Qasem, N.; Ben-Mansour, R.; Habib, M.A. An efficient CO₂ adsorptive storage using MOF-5 and MOF-177. *Appl. Energy* **2018**, *210*, 317–326. [CrossRef]
65. Montazerolghaem, M.; Aghamiri, S.F.; Talaie, M.R.; Tangestaninejad, S. A comparative investigation of CO₂ adsorption on powder and pellet forms of MIL-101. *J. Taiwan Inst. Chem. Eng.* **2017**, *72*, 45–52. [CrossRef]
66. Zhao, Z.; Li, Z.; Lin, J. Adsorption and Diffusion of Carbon Dioxide on Metal–Organic Framework (MOF-5). *Ind. Eng. Chem. Res.* **2009**, *48*, 10015–10020. [CrossRef]
67. Poirier, E.; Chahine, R.; Bénard, P.; Lafi, L.; Dorval-Douville, G.; Chandonia, P.A. Hydrogen Adsorption Measurements and Modeling on Metal-Organic Frameworks and Single-Walled Carbon Nanotubes. *Langmuir* **2006**, *22*, 8784–8789. [CrossRef]
68. Peedikakkal, A.M.P.; Al-Betar, A.R.; Al-Mousa, A.H. Conductivity Enhancement of Mofs via Development of Mofpolymer Composite Material. U.S. Patent 20200291045A1, 17 September 2020.

69. Zacharia, R.; Fernando Gomez, L.; Chahine, R.; Cossement, D.; Benard, P. Thermodynamics and kinetics of CH₄/CO₂ binary mixture separation by metal-organic frameworks from isotope exchange and adsorption breakthrough. *Microporous Mesoporous Mater.* **2018**, *263*, 165–172. [CrossRef]
70. Viditha, V.; Rao, M.V.; Srilatha, K.; Himabindu, V.; Yerramilli, A. A study on metal organic framework (MOF-177) synthesis, characterization and hydrogen adsorption–desorption cycles. *Int. J. Energy Environ.* **2013**, *4*, 127–132.
71. Saha, D.; Deng, S. Synthesis, characterization and hydrogen adsorption in mixed crystals of MOF-5 and MOF-177. *Int. J. Hydrogen Energy* **2009**, *34*, 2670–2678. [CrossRef]
72. Férey, G.; Mellot-Draznieks, C.; Serre, C.; Millange, F.; Dutour, J.; Surlé, S.; Margiolaki, I. A Chromium Terephthalate-Based Solid with Unusually Large Pore Volumes and Surface Area. *Science* **2005**, *309*, 2040–2042. [CrossRef] [PubMed]
73. Bhattacharjee, S.; Chena, C.; Ahn, W.S. Chromium terephthalate metal–organic framework MIL-101: Synthesis, functionalization, and applications for adsorption and catalysis. *RSC Adv.* **2014**, *4*, 52500. [CrossRef]
74. Wurzbacher, J.A. Development of a Temperature-Vacuum Swing Process for CO₂ Capture from Ambient Air. Ph.D. Thesis, ETH Zurich, Zurich, Switzerland, 2015.
75. Eytipe. Modelling of CO₂ Using Metal Organic Frameworks. Master’s Thesis, King Fahd University, Dhahran, Arabia Saudita, 2015.
76. Kaskel, S. *The Chemistry of Metal Organic Frameworks*; Wiley: Hoboken, NJ, USA, 2016.
77. Goyal, P.; Purdue, M.; Farooq, S. Adsorption and Diffusion of N₂ and CO₂ and Their Mixture on Silica Gel. *Ind. Eng. Chem. Res.* **2019**, *58*, 19611–19622. [CrossRef]
78. Climeworks. 2020. Available online: www.climeworks.com (accessed on 1 December 2020).
79. Gebald, C.; Piatkowski, N.; Ruesch, T.; Wurzbacher, J.A. Low-Pressure Drop Structure of Particle Adsorbent Bed for Adsorption Gas Separation Process. WO Patent 2014/170184 A1, 23 October 2014.
80. Buijs, W.; de Flart, S. Direct Air Capture of CO₂ with an Amine Resin: A Molecular Modeling Study of the CO₂ Capturing Process. *Ind. Eng. Chem. Res.* **2017**, *56*, 12297–12304. [CrossRef]
81. Knox, J.C.; Ebner, A.D.; LeVan, M.D.; Coker, R.F.; Ritter, J.A. Limitations of Breakthrough Curve Analysis in Fixed-Bed Adsorption. *Ind. Eng. Chem. Res.* **2016**, *55*, 4734–4748. [CrossRef] [PubMed]
82. Morales-Ospino, R.; Santiago, R.G.; Siqueira, R.M.; de Azevedo, D.C.S.; Bastos-Neto, M. Assessment of CO₂ desorption from 13X zeolite for a prospective TSA process. *Adsorption* **2020**, *26*, 813–824. [CrossRef]
83. Perry, R.H. *Perry’s Chemical Engineerings’ Handbook*; McGraw-Hill: New York, NY, USA, 1999.
84. Poundsterlinglive. 2021. Available online: <https://www.poundsterlinglive.com/bank-of-england-spot/historical-spot-exchange-rates/usd/USD-to-CHF-1993> (accessed on 1 July 2021).
85. Mason, J.A.; Sumida, K.; Herm, Z.R.; Krishna, R.; Long, J.R. Evaluating metal–organic frameworks for post-combustion carbon dioxide capture via temperature swing adsorption. *Energy Environ. Sci.* **2011**, *4*, 3030–3040. [CrossRef]
86. Zhang, Z.; Huang, S.; Xian, S.; Xi, H.; Li, Z. Adsorption Equilibrium and Kinetics of CO₂ on Chromium Terephthalate MIL-101. *Energy Fuels* **2011**, *25*, 835–842. [CrossRef]
87. Keller, J.U. *Gas Adsorption Equilibria: Experimental Methods and Adsorptive Isotherms*; Springer: New York, NY, USA, 2005.
88. Yu, Q.; Brilman, D.W.F. Design strategy for CO₂ adsorption from ambient air using a supported amine based sorbent in a fixed bed reactor. *Energy Procedia* **2017**, *114*, 6102–6114. [CrossRef]
89. Zhang, W.; Liu, H.; Sun, Y.; Cakstins, J.; Sun, C.-G.; Snape, C. Parametric study on the regeneration heat requirement of an amine-based solid adsorbent process for post-combustion carbon capture. *Appl. Energy* **2016**, *168*, 394–405. [CrossRef]
90. Wurzbacher, J.A.; Gebald, C.; Steinfeld, A. Separation of CO₂ from air by temperature-vacuum swing adsorption using diamine-functionalized silica gel. *Energy Environ. Sci.* **2011**, *4*, 3584–3592. [CrossRef]
91. Huck, J.M.; Lin, L.-C.; Berger, A.H.; Shahrak, M.N.; Martin, R.L.; Bhowan, A.S.; Haranczyk, M.; Reuter, K.; Smit, B. Evaluating different classes of porous materials for carbon capture. *Energy Environ. Sci.* **2014**, *7*, 4132–4146. [CrossRef]
92. Peter, M.S.; Timmerhaus, K.D. *Plant Design and Economics for Chemical Engineering*; McGraw-Hill: New York, NY, USA, 1991.
93. Matches. 2020. Available online: <http://www.matches.com/equipcost/Default.html> (accessed on 1 December 2020).
94. Towerling Skills. 2021. Available online: <https://www.toweringskills.com/financial-analysis/cost-indices/> (accessed on 1 July 2021).
95. Danaci, D.; Bui, M.; Mac Dowell, N.; Petit, C. Exploring the limits of adsorption-based CO₂ capture using MOFs with PVSA—from molecular design to process economics. *Mol. Syst. Des. Eng.* **2019**, *5*, 212–231. [CrossRef]
96. Bauer, C.; Cox, B.; Heck, T.; Zhang, X. *Potentials, Costs and Environmental Assessment of Electricity Generation Technologies*; PSI, Technology Assessment Group: Villigen, Switzerland, 2019.
97. SDH. 2017. Available online: <https://www.solar-district-heating.eu/switzerland-plans-for-solar-district-heating-pilot-system/> (accessed on 13 May 2021).
98. Gebelman, A. Adsorption Basics: Part 1. 2017. Available online: https://www.aiche.org/sites/default/files/docs/pages/adsorption_basics_part_1.pdf (accessed on 1 December 2020).
99. Papurello, D.; Gandiglio, M.; Lanzini, A. Experimental Analysis and Model Validation on the Performance of Impregnated Activated Carbons for the Removal of Hydrogen Sulfide (H₂S) from Sewage Biogas. *Processes* **2019**, *7*, 548. [CrossRef]
100. Patel, S.M. Evaluation of Mass Transfer Rate in Column of Small Lilsx Particle. Master’s Thesis, Cleveland State University, Cleveland, OH, USA, 2017.

101. Bahrun, M.H.V.; Bono, A.; Dzilrazman, N.K.; Kamin, Z. Recovery of Minor Palm Oil Compounds Using Packed Bed Adsorption Column. *J. Bahan Alam Terbarukan* **2020**, *9*, 21–29. [[CrossRef](#)]
102. Naksusuk, S.; Tangsathitkulchai, C. Carbon Dioxide Capture in a Fixed Bed of Coconut Shell Activated Carbon Impregnated With Sodium Hydroxide: Effects of Carbon Pore Texture and Alkali Loading. *Eng. J.* **2019**, *23*, 29–48. [[CrossRef](#)]
103. Pirngruber, G.D.; Leinekugel-Le-Cocq, D. Design of a Pressure Swing Adsorption Process for Postcombustion CO₂ Capture. *Ind. Eng. Chem. Res.* **2013**, *52*, 5985–5996. [[CrossRef](#)]
104. Smith, R. *Chemical Process Design and Integration*; McGraw Hill: New York, NY, USA, 2005.
105. Wurzbacher, J.A.; Gebald, C.; Piatkowski, N.; Steinfeld, A. Concurrent Separation of CO₂ and H₂O from Air by a Temperature-Vacuum Swing Adsorption/Desorption Cycle. *Environ. Sci. Technol.* **2012**, *46*, 9191–9198. [[CrossRef](#)] [[PubMed](#)]
106. Elfvinga, J.; Kauppinena, J.; Jegoroffa, M.; Ruuskanenb, V.; Järvinenb, L.; Sainioc, T. Experimental comparison of regeneration methods for CO₂ concentration from air using amine-based adsorbent. *Chem. Eng. J.* **2021**, *404*, 126337. [[CrossRef](#)]
107. Towler, G.; Sinnott, R.K. *Chemical Engineering Design: Principles, Practice and Economics of Plant and Process Design*; BH: Oxford, UK, 2012.
108. Primo, J. 2012. Available online: <https://pdhonline.com/courses/m385/m385content.pdf> (accessed on 1 December 2020).
109. House, K.Z.; Baclig, A.C.; Ranjan, M.; van Nierop, E.A.; Wilcox, J.; Herzog, H.J. Economic and energetic analysis of capturing CO₂ from ambient air. *Proc. Natl. Acad. Sci. USA* **2011**, *108*, 20428–20433. [[CrossRef](#)]
110. Krekel, D.; Samsun, R.C.; Peters, R.; Stolten, D. The separation of CO₂ from ambient air—A techno-economic assessment. *Appl. Energy* **2018**, *218*, 361–381. [[CrossRef](#)]
111. Carbonbrief. 2020. Available online: www.carbonbrief.org/swiss-company-hoping-capture-1-global-co2-emissions-2025 (accessed on 1 December 2020).
112. Narula, K.; Filho, F.D.O.; Chambers, J.; Romano, E.; Hollmuller, P.; Patel, M.K. Assessment of techno-economic feasibility of centralised seasonal thermal energy storage for decarbonising the Swiss residential heating sector. *Renew. Energy* **2020**, *161*, 1209–1225. [[CrossRef](#)]